Contrasts between Urban and Rural Climate in CCSM4 CMIP5 Climate Change Scenarios

KEITH OLESON

National Center for Atmospheric Research, Boulder, Colorado*

(Manuscript received 17 February 2011, in final form 7 July 2011)

ABSTRACT

A new parameterization of urban areas in the Community Climate System Model version 4 (CCSM4) allows for simulation of temperature in cities where most of the global population lives. CCSM4 Coupled Model Intercomparison Project phase 5 (CMIP5) simulations [Representative Concentration Pathway (RCP) 2.6, 4.5, and 8.5] are analyzed to examine how urban and rural areas might respond differently to changes in climate. The urban heat island (UHI), defined as the urban minus rural air temperature, is used as a metric. The average UHI at the end of the twenty-first century is similar to present day in RCP2.6 and RCP4.5, but decreases in RCP8.5. Both the daytime and nocturnal UHIs decrease in RCP8.5, but the decrease in the daytime UHI is larger and more uniform across regions and seasons than in the nocturnal UHI. This is caused by changes in evaporation that warm the rural surface more than the urban. There is significant spatial and seasonal variability in the response of the nocturnal UHI caused mainly by changes in the rural surface. In Europe, the response to climate change of rural leaf–stem area in summer and clouds and rural soil moisture in winter explains the majority of this variability. Climate change increases the number of warm nights in urban areas substantially more than in rural areas. These results provide evidence that urban and rural areas respond differently to climate change. Thus, the unique aspects of the urban environment should be considered when making climate change projections, particularly since the global population is becoming increasingly urbanized.

1. Introduction

Urban areas are home to more than 50% of the world's people. By 2050, this number is expected to be close to 70% (United Nations 2009). Many of the sources of global problems such as climate change, pollution, crime, disease, and poverty originate from or are exacerbated by human activities concentrated within urban areas (Bettencourt and West 2010). In growing recognition of these issues, an increasing amount of interdisciplinary research is aimed at understanding the urban environment and significant resources are being allocated to devising solutions to these problems. For example, scientists, engineers, and urban decision-makers are beginning to work together to address the potential interactions between urban areas and climate change and to consider adaptation and mitigation strategies (Hunt et al. 2007; Rosenzweig et al. 2010; Coutts et al. 2010).

The field of urban climatology has a long and rich history of research focused on observing, modeling, and understanding urban effects on climate and weather (e.g., as reviewed by Landsberg 1981; Oke 1988; Arnfield 2003; Collier 2006; Seto and Shepherd 2009). The urban heat island (UHI), a phenomenon describing the fact that urban areas are generally warmer than the surrounding rural areas was first recognized by Luke Howard in 1820 as described by Landsberg (1981) in his authoritative review of the field of urban climatology (Oke 1991). The causes of the UHI were investigated in a series of investigations by Oke and others using observations and numerical modeling (e.g., Oke 1981, 1982; Oke et al. 1991).

The average UHI for a midlatitude city is 1°–3°C but may reach up to 12°C at night under optimal conditions (Oke 1997) and is generally largest during the summer season (Karl et al. 1988; Klysik and Fortuniak 1999). In the tropics, seasonal variations of the UHI are evidently

* The National Center for Atmospheric Research is sponsored by the National Science Foundation.

Corresponding author address: Keith Oleson, National Center for Atmospheric Research, 1850 Table Mesa Drive, Boulder, CO 80305.
E-mail: oleson@ucar.edu

DOI: 10.1175/JCLI-D-11-00098.1

more related to urban–rural surface moisture characteristics with higher intensities during the dry season (Roth 2007). The maximum UHI appears to depend slightly on latitude with values of 4°C in the tropics and about 6°C at midlatitudes, partly due to differences in anthropogenic heat generation and radiation balance (Wienert and Kuttler 2005). Zhang et al. (2010) report remotely sensed globally averaged daytime skin temperature UHIs of 2.6°C in summer and 1.4°C in winter.

Mesoscale models have been applied to the study of the UHI and more generally urban climate. Some of the earliest simulations were applied to studies of the urban energy balance (Myrup 1969) and urban-induced circulation patterns (Bornstein 1975). Over the next 30 years, increasingly sophisticated urban parameterizations were used (see reviews by Bornstein 1986; Brown 2000; Masson 2006). Most recently, explicit representations of the effects of individual urban components (e.g., roofs, walls, and roads) on the urban energy budget have been implemented (Mills 1997; Masson 2000; Martilli et al. 2002; Chen et al. 2010).

Climate change scientists working at global scales are now beginning to apply lessons learned from these observational and modeling efforts and devote significant modeling and computing resources to develop an understanding of urban climate and its possible interactions with climate change. Global climate modeling groups at the Hadley Centre and the National Center for Atmospheric Research have implemented urban models within the land surface model components of their respective climate models (Best et al. 2006; Oleson et al. 2008a) and have used these models to study how UHIs might change in the future (McCarthy et al. 2010a; Oleson et al. 2010a). There are limitations to representing urban areas within global climate models (see discussion in section 6), but such an integrated model means that the response of urban areas can be studied under the full range of atmospheric conditions produced from future climate scenarios of interest.

McCarthy et al. (2010a) examined changes in the UHI under doubled CO_2 conditions and anthropogenic heat scenarios using the Hadley Center Atmospheric Model version 3 (HadAM3) atmosphere-only (prescribed sea surface temperatures) climate model. Oleson et al. (2010a) used the Community Atmosphere Model version 3.5 (CAM3.5) coupled to the Community Land Model–Urban (CLMU) to investigate UHI characteristics for present day through the end of the twenty-first century under an Intergovernmental Panel on Climate Change (IPCC) Fourth Assessment Report (AR4) A2 scenario. One of the common conclusions of these two papers was that the UHI is not necessarily static under climate change, thus making the argument for explicit representation of urban areas within climate models. Here, the work of Oleson et al. (2010a) is expanded to analyze climate change simulations being performed for the IPCC AR5 as part of the Coupled Model Intercomparison Project phase 5 (CMIP5; Taylor et al. 2009). Specifically, the response of urban and rural areas is contrasted for present-day conditions and three plausible trajectories of future climate conditions [Representative Concentration Pathways (RCPs): RCP8.5, RCP4.5, and RCP2.6; Moss et al. (2010)].

Sections 2, 3, and 4 describe the models, simulations, and analysis methods, respectively. Several aspects of urban and rural climate are examined including time series of urban and rural air temperature (section 5a), spatial and seasonal variability in changes in urban and rural air temperature (section 5b), and interactions of changes in climate with urban space heating and air conditioning (section 5c). In recognition of the fact that changes in absolute temperature and in particular changes in extremes may be important in determining heat-related mortality (Gosling et al. 2009), section 5d presents an analysis of changes in hot days and warm nights. Section 5e presents an analysis of processes responsible for changes in urban and rural air temperature and thus the heat island. Section 6 summarizes and discusses the results in the context of model and dataset limitations.

2. Model description

The Community Climate System Model version 4 (CCSM4) is described fully in Gent et al. (2011). CCSM4 consists of atmosphere (Neale et al. 2011), ocean (Danabasoglu et al. 2012), sea ice (Hunke and Lipscomb 2008; Holland et al. 2012), and land components that are linked together through a coupler that exchanges state and flux information between components. The land component is the Community Land Model (CLM4; Lawrence et al. 2011; Oleson et al. 2010b; Lawrence et al. 2012). Included in the CLM4 is a parameterization of an urban surface type that is modeled as a separate landunit within a model grid cell (CLMU; Oleson et al. 2008a,b), in addition to vegetated, glacier, wetland, and lake landunits (Fig. 1). A full technical description of CLMU can be found in Oleson et al. (2010c), a brief description is provided here for convenience.

The urban land unit has the following five components: roof, sunlit wall, shaded wall, and pervious (e.g., to represent residential lawns, parks) and impervious (e.g., to represent roads, parking lots, sidewalks) canyon floor (these components are denoted as columns in the CLM subgrid structure shown in Fig. 1). Following the CLM4 structural configuration for snow–soil, each urban component is divided into 15 layers for temperature and hydrology calculations and up to five

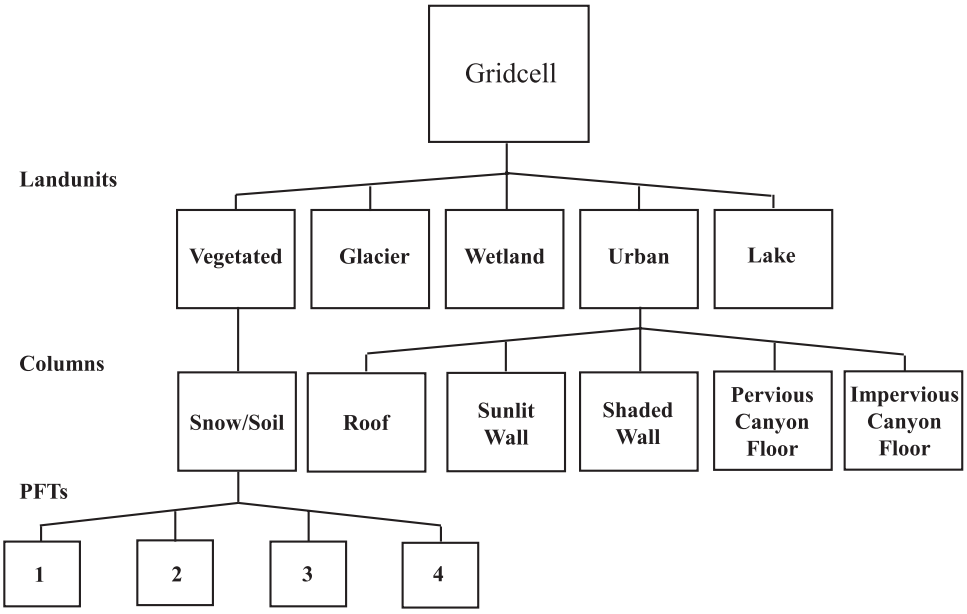

FIG. 1. The CLM subgrid hierarchy emphasizing the vegetated and urban landunits. Grid cells are composed of landunits, snow–soil–urban columns, and plant functional types (PFTs). Four PFTS are shown here but up to 16 possible PFTs that differ in physiology and structure may coexist on a single column. Reproduced from Fig. 1 of Oleson et al. (2010a) with permission from John Wiley & Sons, Inc.

additional layers for snow based on snow depth. The urban components are arranged in an ''urban canyon'' configuration (Oke 1987) in which the canyon geometry is described by building height (H) and street width (W) (Fig. 2).

Turbulent [sensible ($Q_{H,\mathrm{us}}$) and latent heat ($Q_{E,\mathrm{us}}$)] and storage ($Q_{S,\mathrm{us}}$) heat fluxes, and surface ($T_{\mathrm{us},s}$) and internal temperatures ($T_{\mathrm{us},1\cdots15}$) are determined for each urban surface (us) (Fig. 2). The interior boundary conditions for roofs and walls are determined by an interior building temperature (T_{iB}) held between prescribed minimum and maximum temperatures ($T_{\mathrm{iB,min}}$ and $T_{\mathrm{iB,max}}$), thus simulating space heating and air conditioning (HAC) fluxes. Hydrology on the roof and canyon floor is simulated and walls are hydrologically inactive. A snowpack can form on the active surfaces. Liquid water is allowed to pond on these surfaces, which supports evaporation. Snowmelt water or water in excess of the maximum ponding depth runs off (R_{roof}, R_{imprvrd}). The hydrology for the pervious canyon floor is parameterized similarly to CLM4 soil (Oleson et al. 2010b). However, the evaporative processes associated with vegetation within the urban canyon are not explicitly represented (i.e., evaporation of canopy intercepted water and transpiration). Instead, evaporation is parameterized by a bulk scheme in which evaporation is a function of the wetness of the entire soil column and water is removed from each soil layer.

Heat emissions produced by anthropogenic activities (wasteheat) are a contributor to the UHI. Globally this flux is small compared to greenhouse gas forcing, one estimate is that it is on the order of 0.03 W m^{-2} (Flanner 2009), however, within cities it can be a significant and even dominant component of the local urban energy budget (Ichinose et al. 1999). Sources of wasteheat include human metabolism, vehicles, commercial and residential buildings, industry, and power plants (Sailor 2010). Global spatially explicit datasets of wasteheat are now becoming available (Flanner 2009; Allen et al. 2011), and thus wasteheat could be prescribed as a flux in the urban energy budget. However, wasteheat varies strongly with climate and it is desirable in a climate model to account for this dependence (Hadley et al. 2006). Here, an anthropogenic source of wasteheat ($Q_{H,\mathrm{waste}}$) (Fig. 2) from inefficiencies in the HAC systems is added to the net heat flux for the canyon floor and thus contributes to the UHI (Oleson et al. 2010a). Heat removed by air conditioning is added to the canyon floor heat flux as well.

The heat and moisture fluxes from each surface interact with each other through a bulk air mass that represents air in the urban canopy layer (UCL) for which temperature (T_s), humidity (q_s), and wind speed (u_s) are forecasted (Fig. 2). The urban model produces sensible heat, latent heat, and momentum fluxes, and emitted longwave and reflected solar radiation ($Q_H, Q_E, \tau, L\uparrow, S\uparrow$; Fig. 2). These are area averaged with fluxes from nonurban landunits

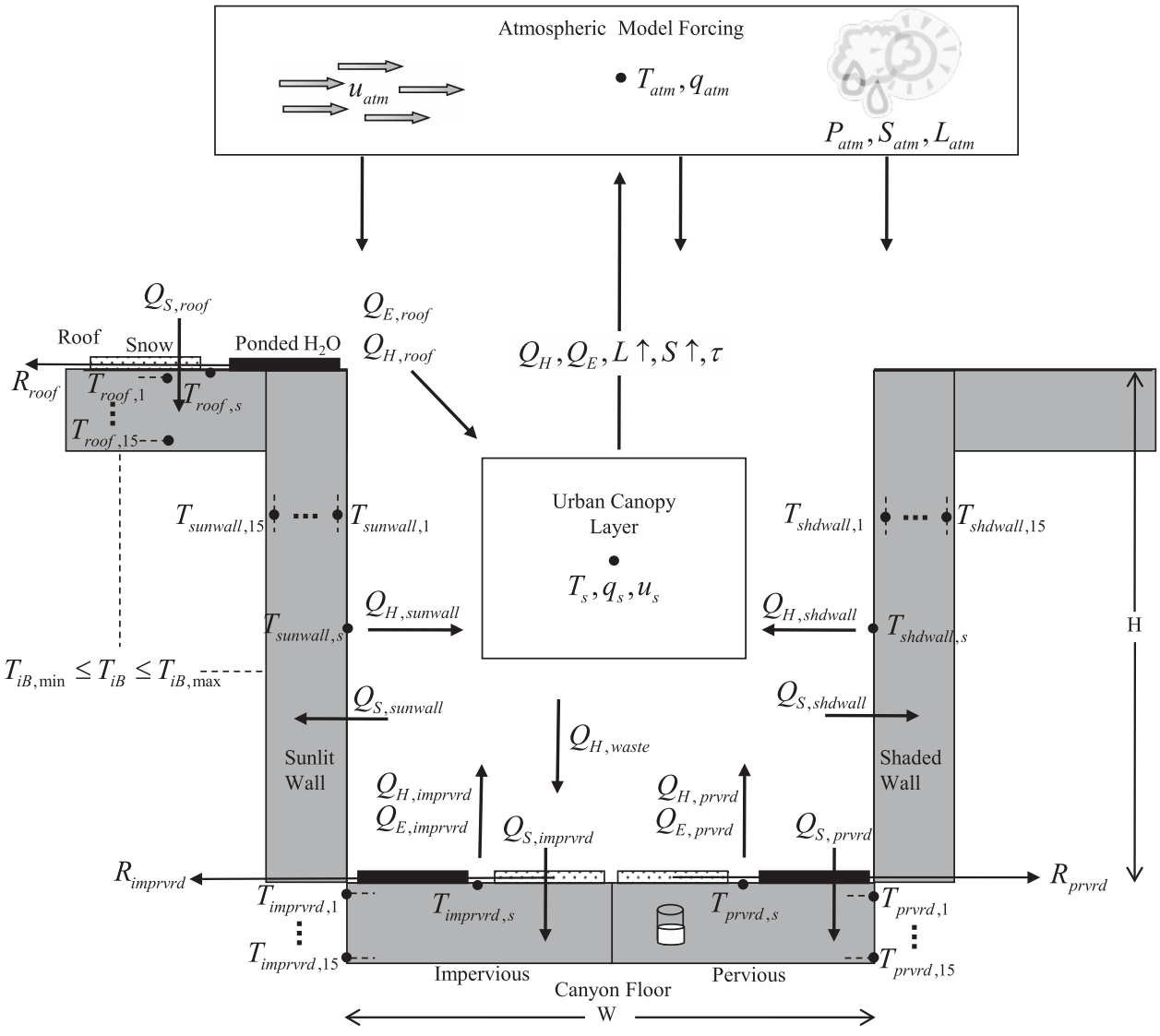

FIG. 2. Schematic representation of the urban landunit (modified from Fig. 2 of Oleson et al. 2008a). See section 2 for description of notation. Incident, reflected, and net solar and longwave radiation are calculated for each individual surface but are not shown for clarity.

(e.g., vegetation, lakes) to supply gridcell-averaged fluxes to the atmospheric model. The atmospheric model provides the urban model with air temperature and humidity, wind speed, precipitation, and downward solar and longwave radiation ($T_{\rm atm}, q_{\rm atm}, u_{\rm atm}, P_{\rm atm}, S_{\rm atm}, L_{\rm atm}$; Fig. 2).

Present-day urban extent and urban properties are provided by the global dataset developed by Jackson et al. (2010). At the spatial resolution of the simulations performed here (section 3), urban areas occupy about 0.6% of the global land surface. Urban area is typically a small percentage of the land fraction of the grid cells (0.1%–10%) but may occupy up to 100% in coastal grid cells with a small land fraction. Urban properties include thermal (e.g., heat capacity and thermal conductivity), radiative (e.g., albedo and emissivity), and morphological (e.g., height to width ratio, roof fraction, average building height, and pervious fraction of canyon floor) properties, and building interior minimum and maximum temperatures based on climate and socioeconomic considerations. These properties are defined uniquely for 33 geographical regions which represent variations in urban morphology and building construction (Jackson et al. 2010). Details of the specific implementation of this dataset within CCSM4 can be found in Oleson et al. (2010a,c). An important aspect of this implementation is that the model is currently limited to a single urban landunit per grid cell, instead of up to four urban density types provided by the dataset (tall building district, high, medium, and low density). This is chosen to be the

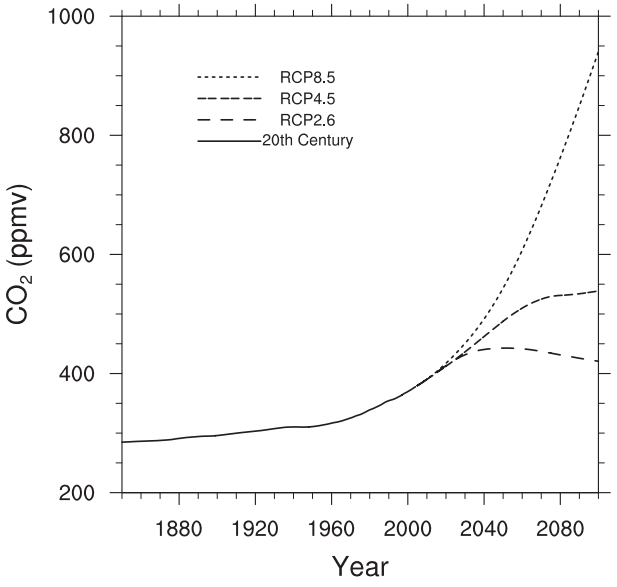

FIG. 3. Global CO_2 concentrations (ppmv) for the twentieth-century and RCP8.5, RCP4.5, and RCP2.6 simulations.

dominant density type by area which means that urban areas globally are almost exclusively medium density. The properties of the medium density type do vary spatially but general characteristics are that buildings are 1 to 3 stories tall, the building height to street width ratio is 0.5–2.0, and a significant fraction of the canyon floor is pervious.

The performance of the model has been evaluated against measured fluxes and temperatures from urban flux tower sites for short observation periods (less than a week) by Oleson et al. (2008a) and Oleson et al. (2010c) and reproduces known qualitative features of urban climatology, including UHIs (Oleson et al. 2008b, 2010a). Evaluation of the present day UHI and its latitudinal and seasonal variability has been performed by Oleson et al. (2008b), Oleson et al. (2010a), and also by Jackson et al. (2010). The model is also a participant in the International Urban Energy Balance Models Comparison Project (Grimmond et al. 2010, 2011). In the project's second phase, the model was evaluated for its ability to reproduce urban energy balance fluxes over a 12-month period. At stage 4 when all site data were made available, the model's performance ranked 12th, 5th, and 8th out of 31 models in root-mean-square error for hourly fluxes of net radiation, sensible heat, and latent heat, respectively (model 43 in Grimmond et al. 2011).

3. Description of climate simulations

The climate simulations analyzed here have been conducted with CCSM4 following the protocol of CMIP5 (Taylor et al. 2009). Model output from ensemble members of the twentieth-century simulation and three RCP simulations (RCP8.5, RCP4.5, and RCP2.6; Moss et al. 2010) are analyzed. The twentieth-century simulations are run from 1850–2005 (five ensemble members) and are initialized from various years of a CCSM4 preindustrial (1850) control simulation. The RCP simulations (five ensemble members for each RCP) are initialized from the twentieth-century ensemble members and run for 2005–2100. RCP8.5 is a high emissions scenario with radiative forcing reaching 8.5 W m^{-2} near 2100. RCP4.5 is a medium mitigation scenario with radiative forcing stabilizing at 4.5 W m^{-2} after 2100. RCP2.6 results in radiative forcing peaking at 3.1 W m^{-2} by midcentury, returning to 2.6 W m^{-2} by 2100. Figure 3 shows time series of global CO_2 concentrations for the twentieth-century and each RCP. CO_2 levels reach 940, 538, and 421 ppmv by 2100 in RCP8.5, RCP4.5, and RCP2.6, respectively.

The forcings in these simulations include prescribed changes in solar irradiance, greenhouse gases (CO_2, CH_4, N_2O, O_3, CFCs), natural and anthropogenic aerosol burden, aerosol (black carbon and dust) and nitrogen deposition, and land cover change (e.g., conversion of natural vegetation to cropland, abandonment of cropland) including harvest of wood. In addition, the carbon–nitrogen (CN) component of CLM4 is active, which means that leaf and stem area and canopy height of vegetated surfaces are determined prognostically in response to changes in climate. Thus, the energy balance and near-surface climate of the rural landunit is not only influenced by changes in atmospheric forcing (i.e., precipitation, incoming solar and longwave radiation, and air temperature, humidity, and wind at the lowest atmospheric model layer), CO_2 (through the response of plant stomata), and nitrogen and aerosol deposition (which affect the carbon–nitrogen cycle and snow albedo, respectively), but also by changes in the rural surface itself. For instance, prescribed changes in land cover changes the composition of plant functional types (PFTs) within the grid cell. Changes in leaf and stem area prognosed by the CN model affect energy and water balances of the vegetated surface. The energy balance and near-surface climate of the urban landunit in the model is affected only by changes in atmospheric forcing and not by any other factors. In particular, urban fractional area is constant at present-day values, urban properties do not change in time, and the urban areas are not affected by changes in atmospheric CO_2 and nitrogen and aerosol deposition.

One member each of the twentieth-century and RCP8.5 ensembles was rerun to obtain supplementary hourly output. The twentieth-century ensemble member was run for 1986–2005 and the RCP8.5 member was run for 2080–99. These simulations have identical climate compared to the

original simulations. These two simulations allow for an analysis of changes in hot days and warm nights for urban and rural areas and an examination of the diurnal cycle of urban and rural energy balance and temperature. All simulations are run on a 0.9375° latitude by 1.25° longitude grid. Other than time series of air temperature for which results of individual ensemble members are presented, the analysis here uses averages of the ensemble members.

4. Analysis methods

The urban canopy layer air temperature (T_s in Fig. 2) is referred to here as the urban air temperature. A ''rural'' air temperature is defined as the area-weighted average of the 2-m air temperature of the PFTs (including bare soil). The UHI is defined as the difference between the urban and rural air temperatures in each grid cell. This difference is analyzed for daily average (AVG), daily maximum (TMAX), and daily minimum (TMIN) temperature. The urban minus rural TMAX and TMIN are also referred to as the daytime and nocturnal UHIs, respectively. Monthly averaged model output of AVG, TMAX, and TMIN temperatures are used to construct seasonal and annual means.

A strong relation between changes in the nocturnal UHI and the rural diurnal temperature range (DTR) is investigated in section 5e. Correlative and regressive analyses are used to ascribe changes in the rural DTR and the nocturnal UHI (the criterion variables) to changes in atmospheric forcing and surface variables (the predictor variables). Simple correlation coefficients (Pearson correlation coefficient) are calculated between each predictor variable and the criterion variables. The results from multiple linear regression are the standardized partial regression coefficients and represent the relation between a given predictor and the criterion while controlling for all other predictors in the regression equation. The partial correlation coefficient is also calculated and refers to the correlation between a criterion and a predictor after common variance with another predictor has been removed from both the criterion and the predictor of interest (Anderson 2003).

Guided by previous research that indicates DTR and the UHI can be affected by clouds, soil moisture, fog, and changes in landcover (Dai et al. 1999; Zhou et al. 2009; Vautard et al. 2009; Scheitlin and Dixon 2010; Oke 1987), the predictors selected include changes in climate such as humidity (q), wind speed (w), and total cloud fraction (tc), and predictors that describe changes in the urban and rural surface (leaf plus stem area, rural and urban soil moisture, and urban wasteheat) (see Table 5). Downward solar and longwave radiation were also considered initially, however, these predictors are highly correlated with total cloud and can lead to multicollinearity problems in a multiple regression model. Total cloud was selected under the assumption that it captures the effects of changes in both solar and longwave radiation.

Land cover change, in the form of changes in PFT fractions, is prescribed in the RCP simulations. Another type of landcover change occurring in these simulations is the response of the prognostic leaf and stem area in the carbon–nitrogen model to climate change. The predictor lsai is used to account for changes in leaf plus stem area index (m^2 of one-sided leaf plus stem area per m^2 of ground area) due to climate change and prescribed land cover change, which can affect surface energy balance and thus temperature. The predictor $b(r)$ is an indication of soil moisture stress affecting plant transpiration used here as a surrogate for soil moisture for the rural surface, while $b(u)$ indicates soil moisture stress for the urban pervious canyon floor. A decrease in $b(r)$ and $b(u)$ indicates an increase in soil moisture stress and a decrease in soil moisture. The predictor wh is urban wasteheat from HAC processes.

5. Results

a. *Global time series of land, urban, and rural temperature*

Figures 4a–c show 1850–2100 time series of annual mean land, urban, and rural air temperature for all ensemble members of the twentieth-century and RCP simulations. In general, the time series for land follow the time series of CO_2 shown in Fig. 3. The ensemble mean of temperature globally and over land only at present day (1986–2005) is about 1.0° and 1.2°C warmer, respectively, compared to 1850–69 (Table 1). Gent et al. (2011) discuss the trend in global air temperature compared to observations, noting that by 2005 the model anomaly is 0.4°C warmer than observed, likely due to CCSM4 not including the indirect effect of aerosols.

Land temperature increases from present day through the end of the century with the magnitude of increase ordered by the amount of radiative forcing of the RCPs. As compared to present day, the land warms by 1.1°C by midcentury (2046–65), declining to 1.0°C by the end of the century (2080–99) in RCP2.6. The land warms by 1.6° and 2.0°C in RCP4.5, and 2.5° and 4.5°C in RCP8.5 by midcentury and the end of the century, respectively (Table 1). Urban and rural temperatures both increase similarly to land temperature in response to the forcing scenarios (Figs. 4b,c). The model produces an average UHI of 1.35°–1.45°C depending on the time period and

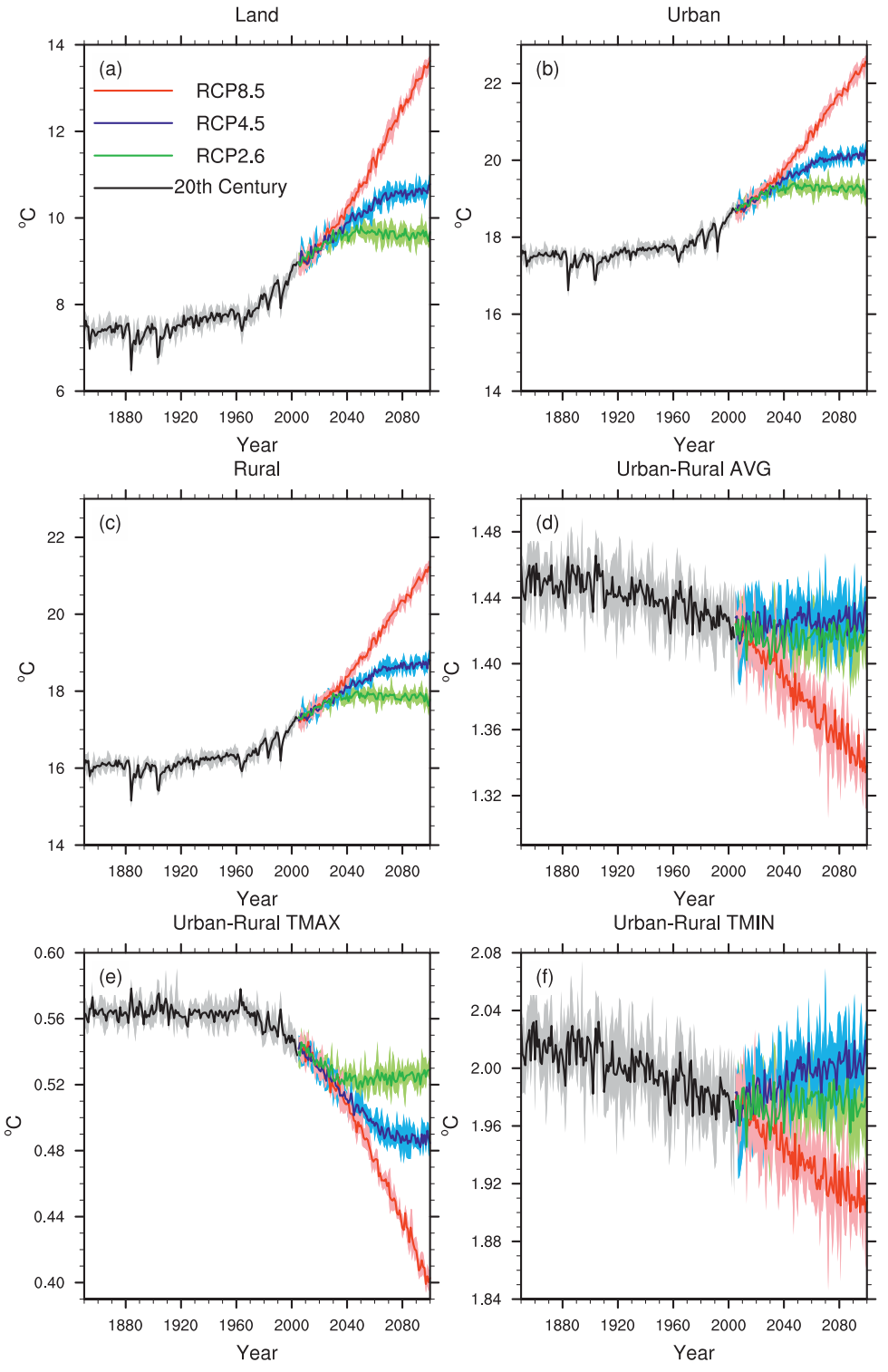

FIG. 4. Time series of annual mean air temperature (°C) over (a) land, (b) urban, and (c) rural areas for 1850–2100 in the twentieth-century and RCP simulations for all ensemble members. Also shown are (d) urban minus rural average (AVG), (e) urban minus rural daily maximum (TMAX), and (f) urban minus rural daily minimum (TMIN) temperatures. Solid lines are the ensemble average. Shaded regions indicate the range of the ensemble members. Land temperatures in (a) represent an average of the grid cell average air temperature over all grid cells that contain land. Rural temperatures represent an average of the rural air temperature over all grid cells that contain urban areas.

TABLE 1. Ensemble mean global, land, urban (U), and rural (R) average 2-m air temperatures (°C) for 1850–69 and 1986–2005 from the twentieth-century simulations, and differences from present day base period 1986–2005 at three future time periods (2011–30, 2046–65, and 2080–99) from the RCP8.5, RCP4.5, and RCP2.6 simulations. Also shown are urban minus rural ($U - R$) average temperature (AVG), $U - R$ daily maximum temperature (TMAX), and $U - R$ daily minimum temperature (TMIN). The urban and rural temperatures represent averages over all grid cells containing urban areas. The future time periods here are the same as those used in AR4 (Meehl et al. 2007).

		Global	Land	U AVG	R AVG	$U - R$ AVG	$U - R$ TMAX	$U - R$ TMIN
Twentieth-century	1850–1869	13.34	7.39	17.51	16.06	1.45	0.56	2.02
	1986–2005	14.30	8.56	18.35	16.93	1.42	0.55	1.98
RCP8.5	2011–30	0.66	0.84	0.72	0.73	1.41	0.53	1.96
	2046–65	1.91	2.48	2.12	2.16	1.38	0.48	1.93
	2080–99	3.48	4.48	3.75	3.82	1.35	0.42	1.91
RCP4.5	2011–30	0.58	0.75	0.65	0.65	1.42	0.53	1.98
	2046–65	1.29	1.65	1.44	1.43	1.43	0.53	2.00
	2080–99	1.62	2.03	1.76	1.75	1.43	0.49	2.00
RCP2.6	2011–30	0.60	0.77	0.68	0.68	1.42	0.53	1.97
	2046–65	0.88	1.12	0.97	0.98	1.41	0.52	1.98
	2080–99	0.85	1.04	0.91	0.91	1.42	0.53	1.97

RCP (Table 1). The UHI is predominantly a nocturnal phenomenon in the model in agreement with observations (Oke and Maxwell 1975; Fortuniak et al. 2005). For example, the present day nocturnal UHI is 3.6 times the daytime UHI (cf. U-R TMIN and TMAX in Table 1).

Oleson et al. (2010a) describe the processes by which UHIs are produced in the model. The partitioning of net radiation into turbulent and storage fluxes is different in urban and rural areas. The urban area stores more heat during the day and releases it later during the day and at night, resulting in a slower cooling rate than rural areas, warmer nocturnal temperatures, and a reduction in the diurnal temperature range, behavior that is supported in a qualitative sense by observations. Lower urban latent heat due to impervious surfaces contributes to warmer urban temperatures as well.

The average UHI declines slightly from 1850 to present day, remains about the same through the end of the twenty-first century in RCP4.5 and RCP2.6, and decreases by 0.07°C at 2080–99 in RCP8.5 compared to present day (Fig. 4d, Table 1). Changes in the daytime UHI (urban minus rural TMAX) (Fig. 4e) appear to be inversely related to changes in atmospheric CO_2. The daytime UHI is steady until about 1960 when it begins to decline as the slope of the CO_2 time series increases. The daytime UHI decreases further in the twenty-first century with the magnitude of the response clearly ordered by radiative forcing. By the end of the twenty-first century, the daytime UHI in RCP8.5 declines by about 24% or 0.13°C from present-day conditions (Table 1). The nocturnal UHI declines in RCP8.5 but remains about the same in RCP4.5 and RCP2.6 compared to present day (Fig. 4f). In contrast to the daytime UHI, the response in the nocturnal UHI is not strictly ordered by radiative forcing. The mean nocturnal UHI in RCP4.5 is slightly higher than in RCP2.6 at the end of the twenty-first century.

The decrease in the UHI over the twentieth-century found here (Figs. 4d–f) is in contrast to many observational studies that note an increase in the UHI (Hansen et al. 2001; Golden 2004; Stone 2007). For example, Stone (2007) found the mean decadal rate of change in the UHI intensity of large U.S. cities between 1951 and 2000 to be 0.05°C. The lack of changes in urban extent and properties in the model explains this discrepancy. These simulations are only an indication of how the UHI changes under static, present-day urban conditions.

b. Spatial and seasonal variability in the heat island

Table 2 shows the present-day average UHI for the regions illustrated in Fig. 5 compared to climate warming in RCP8.5. As noted by Oleson et al. (2010a), the UHI is significant when compared to greenhouse gas warming and so should be accounted for when evaluating the impact of climate change on people. In particular, the present-day average UHI is 32% of the end of the century warming over land in RCP8.5 (Table 1) and is 27%–54% of the warming depending on season and region (Table 2).

Figures 5, 6, and 7 show the spatial and seasonal variability in the response of the average, daytime, and nocturnal UHIs, respectively, to the forcing scenarios at the end of the century compared to present day. There is large spatial and seasonal variability in the change in the average UHI that is generally strongest under the largest radiative forcing (RCP8.5) and smallest with smaller radiative forcing (RCP2.6). However, the patterns of changes in the UHI are fairly similar between the three RCPs, particularly between the two RCPs with the

TABLE 2. Regional averages for the present-day heat island (1986–2005 $U - R$ air temperature), climate change in RCP8.5 (2080–99 minus 1986–2005 land air temperature), and change in the heat island (ΔHI; 2080–99 RCP8.5 $U - R$ minus 1986–2005 $U - R$ air temperature) (°C). Region boundaries (defined as in McCarthy et al. 2010a) are illustrated in Fig. 5: Western North America (WNA), Central America (CAm), South America (SAm), Eastern North America (ENA), Europe (EU), Western Africa (WAf), Middle East (ME), Eastern Africa (EAf), Central Asia (CAs), Eastern Asia (EAs), Australia/New Zealand (ANZ).

	DJF			JJA		
Region	Present-day HI	Climate change	ΔHI	Present-day HI	Climate change	ΔHI
WNA	1.80	3.80	−0.16	1.58	4.49	0.00
ENA	2.04	4.43	−0.17	2.00	4.66	0.11
CAm	1.01	3.35	−0.13	1.06	3.62	−0.11
SAm	1.13	3.65	−0.08	1.60	3.64	−0.01
EU	1.35	2.68	−0.16	1.60	5.06	0.16
WAf	1.86	3.75	−0.11	1.02	3.52	−0.06
ME	1.04	3.80	−0.10	1.32	4.87	0.01
EAf	0.94	3.35	0.01	1.18	3.39	0.00
CAs	2.26	4.19	−0.02	1.14	3.71	−0.06
EAs	1.93	3.69	−0.14	1.29	3.69	−0.10
ANZ	1.07	3.52	−0.09	1.44	3.20	−0.13

strongest radiative forcing (RCP8.5 and RCP4.5). Their pattern correlations are above 0.58 for the AVG, TMAX, and TMIN UHIs in both seasons (Table 3). Correlations are generally weaker between RCP8.5 and RCP2.6 (0.18 to 0.66).

Both increases and decreases in the average and nocturnal UHIs are evident depending on season and geographic location (Fig. 5 and 7). In contrast, the daytime UHI (Fig. 6) decreases quite uniformly across regions, seasons, and RCPs. The largest spatially coherent increases in the nocturnal UHI that appear to be consistent between RCP8.5 and RCP4.5 are in India in boreal winter and in Europe and much of the United States in boreal summer. The largest decreases in the nocturnal UHI are most apparent in boreal winter and occur throughout most of Europe, northern Eurasia, most of the United States, and most of eastern China. Regional averages of changes in the UHI are small relative to greenhouse gas warming and range from −12% to +10% of the present-day UHI in RCP8.5 (Table 2). Locally, however, the changes can be larger. For example, about 15% (boreal winter) and 8% (boreal summer) of the urban areas have changes in the nocturnal UHI larger than 0.5°C in RCP8.5.

c. *Changes in hot days and warm nights*

An important aspect of climate change and its impact on urban and rural populations are the changes in the frequency and intensity of extreme events. In particular, Trenberth et al. (2007) noted an increase in the annual occurrence of hot days and warm nights since 1951, implying an increase in the number of heat waves. Here, changes in the frequency of hot days and warm nights are analyzed from hourly output of single members of the twentieth-century and RCP8.5 ensembles (section 3). Following the analysis in McCarthy et al. (2010a), Fig. 8 shows the average annual frequency of hot days and warm nights for grid cells containing a selected city from each of the 11 regions defined in Fig. 5. These are defined separately for urban and rural areas and 1986–2005 of the twentieth-century simulation and 2080–99 of the RCP8.5 simulation. Hot days are defined as the number of days that the daily maximum air temperature exceeds the 99th percentile of the 1986–2005 rural daily maximum air temperature. Warm nights are defined similarly using the daily minimum air temperature. Note that because of the resolution of the model, the data presented in Fig. 8 for individual cities may include other urban areas. These cities, however, are the major population centers within these grid cells.

McCarthy et al. (2010a) found that climate change (in a doubled CO_2 experiment) increased hot days by a similar amount for urban and rural areas. Here, this is generally the case although there are some exceptions. In Sao Paulo, urban hot days are nearly double those in rural areas likely because of a strong daytime UHI compared to the other cities. In Lagos and Bogata, climate change increases hot days more in rural areas than in urban areas because these cities have daytime cool islands. For the other cities, climate change increases urban hot days by 0 days (Delhi) to 19 days (New York) compared to rural hot days. In contrast, climate change increases the number of warm nights in urban areas substantially more than in rural areas. For example, in London and Delhi, the number of urban warm nights is more than double the number of rural warm nights. In Lagos and Bogata, nearly every night of the year is a warm night in urban areas. McCarthy et al. (2010a) also pointed that simply linearly adding the present-day UHI to future rural climate is not necessarily adequate to

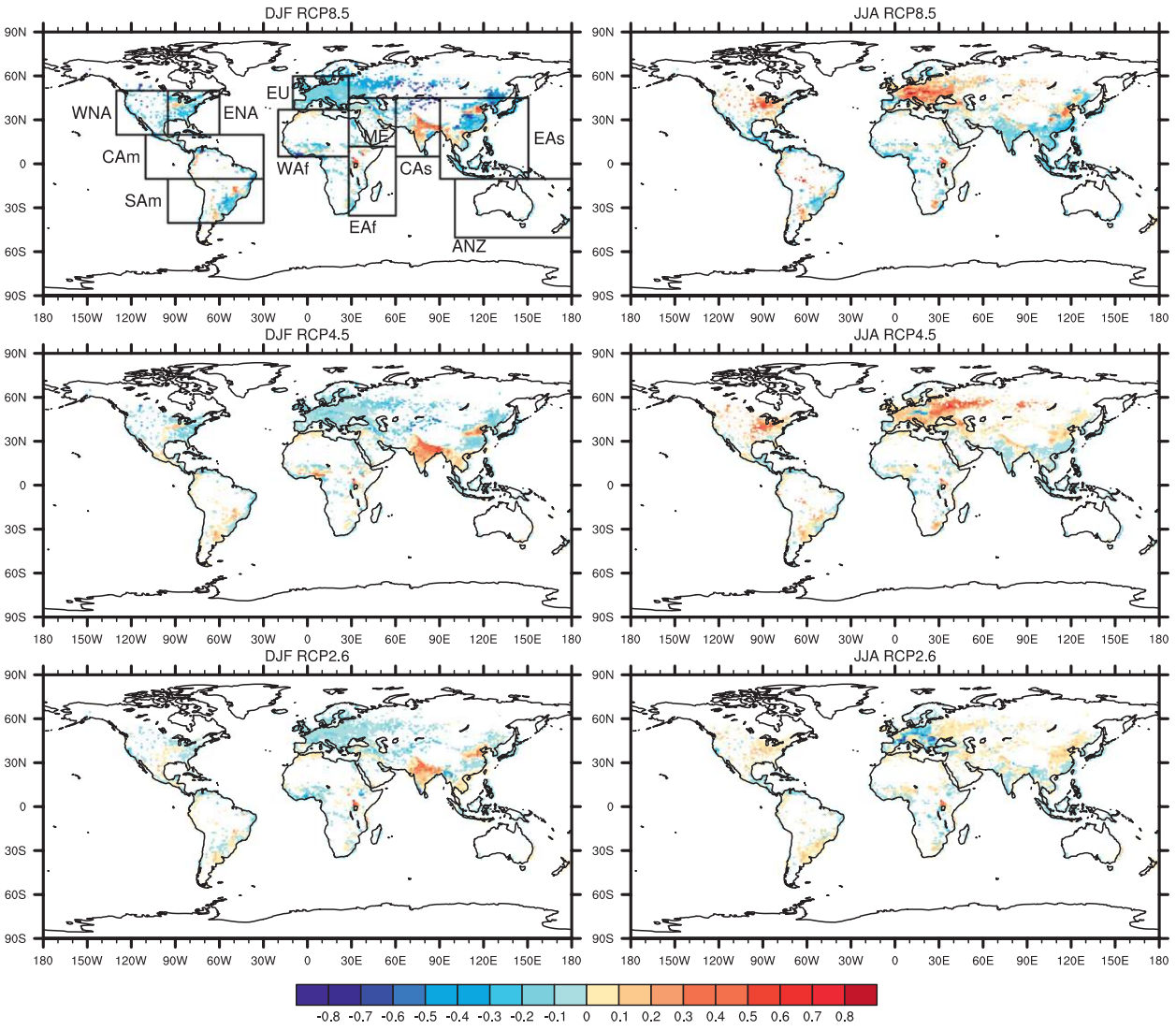

FIG. 5. The 2080–99 minus 1986–2005 (left) December–February (DJF) and (right) June–August (JJA) climatology of urban minus rural average air temperature for (top to bottom) the RCP8.5, RCP4.5, and RCP2.6 simulations. Only differences significant at the 95% level are shown. Also shown are the boundaries for the regions tabulated in Table 2; Western North America (WNA), Central America (CAm), South America (SAm), Eastern North America (ENA), Europe (EU), Western Africa (WAf), Middle East (ME), Eastern Africa (EAf), Central Asia (CAs), Eastern Asia (EAs), Australia–New Zealand (ANZ) (regions defined as in McCarthy et al. 2010a).

estimate urban hot days and warm nights. This is confirmed here by comparing the crosses to the red bars in Fig. 8. Although this method may work for some cities (e.g., Tehran and Nairobi), it is not sufficient for other cities; for example, it overestimates the number of warm nights by 11 in Sydney and underestimates warm nights by 17 in Bogata.

d. Interactions between climate change and urban space heating and air conditioning

Nearly all of the urban space heating, air conditioning, and wasteheat fluxes occur at latitudes of 20°–60°N in the model (Table 4). This is because the urban datasets assume that air conditioning occurs primarily in the United States and because of the lack of urban land at southern latitudes that might require space heating. The air conditioning flux increases and space heating decreases at the end of the century in response to climate warming, with the response ordered by amount of radiative forcing (Table 4). For example, by the end of the century in RCP8.5, global air conditioning flux increases by 0.25 TW (230%) compared to present day and space heating flux decreases by 1.7 TW (35%) (Table 4). At present day, demand for air conditioning is mainly at latitudes of 20°–40°N. The air conditioning flux doubles at these latitudes as climate warms in RCP8.5, and there

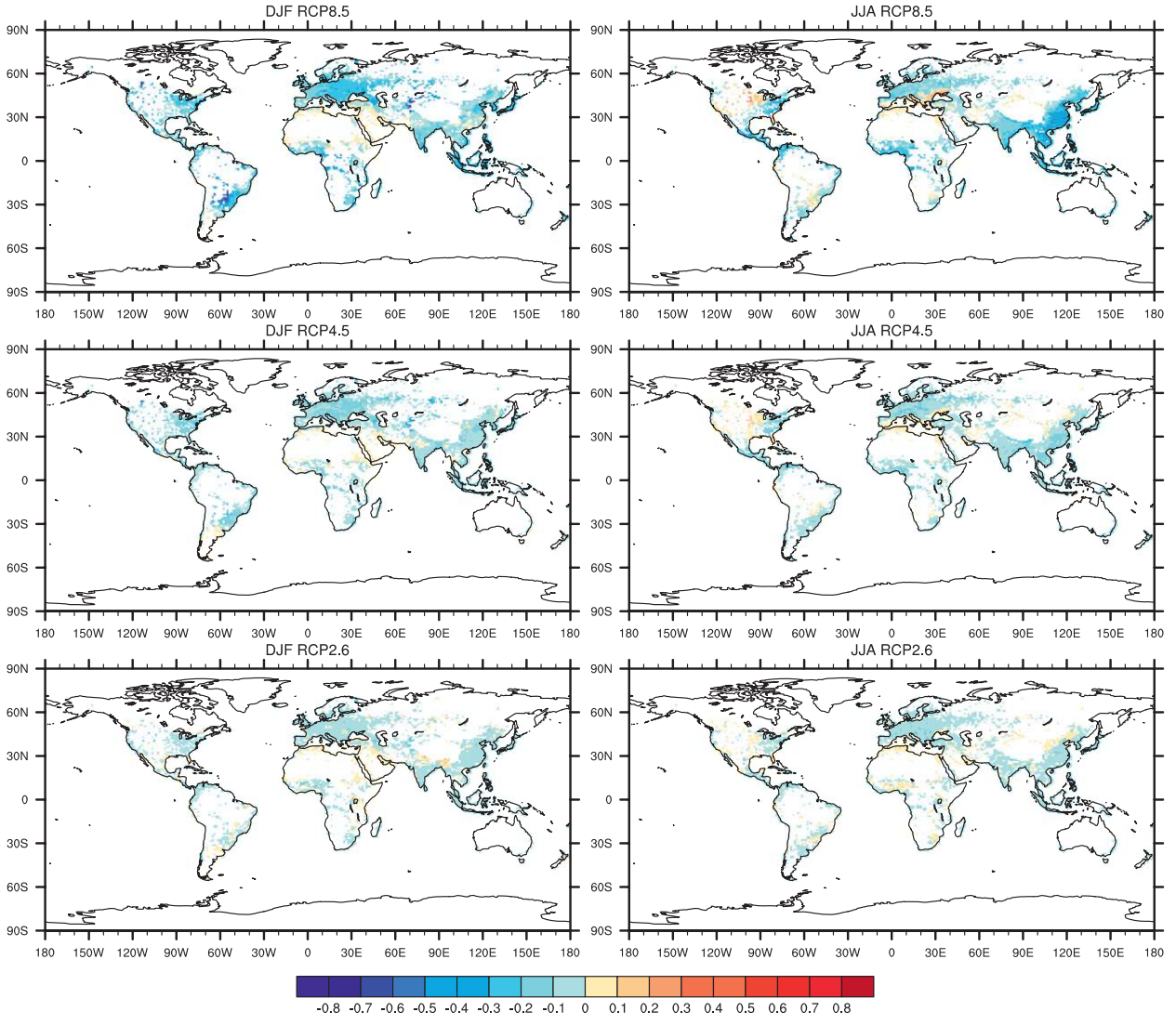

FIG. 6. As in Fig. 5, but for the urban minus rural daily maximum air temperature (daytime heat island).

is a significant increase in air conditioning at latitudes of 40°–60°N. The space heating flux decreases from present day in both latitude bands in all scenarios in response to a warming climate.

Flanner (2009) estimated a global anthropogenic heat flux from nonrenewable sources in 2005 of 0.028 W m^{-2}. As discussed in Oleson et al. (2010a), the amount of anthropogenic heat added to the climate system in the model is due to the nonzero internal boundary condition for roofs and walls plus the air conditioning flux plus the wasteheat from HAC. Calculated in this manner, the simulated present day anthropogenic heat flux is about 6.2 TW (0.012 W m^{-2} distributed globally) or 43% of the Flanner (2009) estimate. If one considers that in the United States, for example, the percentage of total residential and commercial energy used for HAC was 37%–44% (Energy Information Administration 2009, 2008), then the model estimate appears reasonable. On the other hand, the amount of anthropogenic heat can also be calculated as the sum of space heating plus wasteheat (11.3 TW or 0.022 W m^{-2} distributed globally) (Table 4). The heat removed by air conditioning is returned to the urban canyon so that the net air conditioning flux is zero (Oleson et al. 2010c). This estimate is higher because the internal boundary condition is a net sink of energy from the perspective of the climate system (Oleson et al. 2010a). In this case the model estimate of anthropogenic heat is biased high for present day. One reason for this overestimate is that almost all of the urban areas are modeled as medium density, which typically have less well-insulated buildings and therefore require more heating in colder climates (Jackson et al.

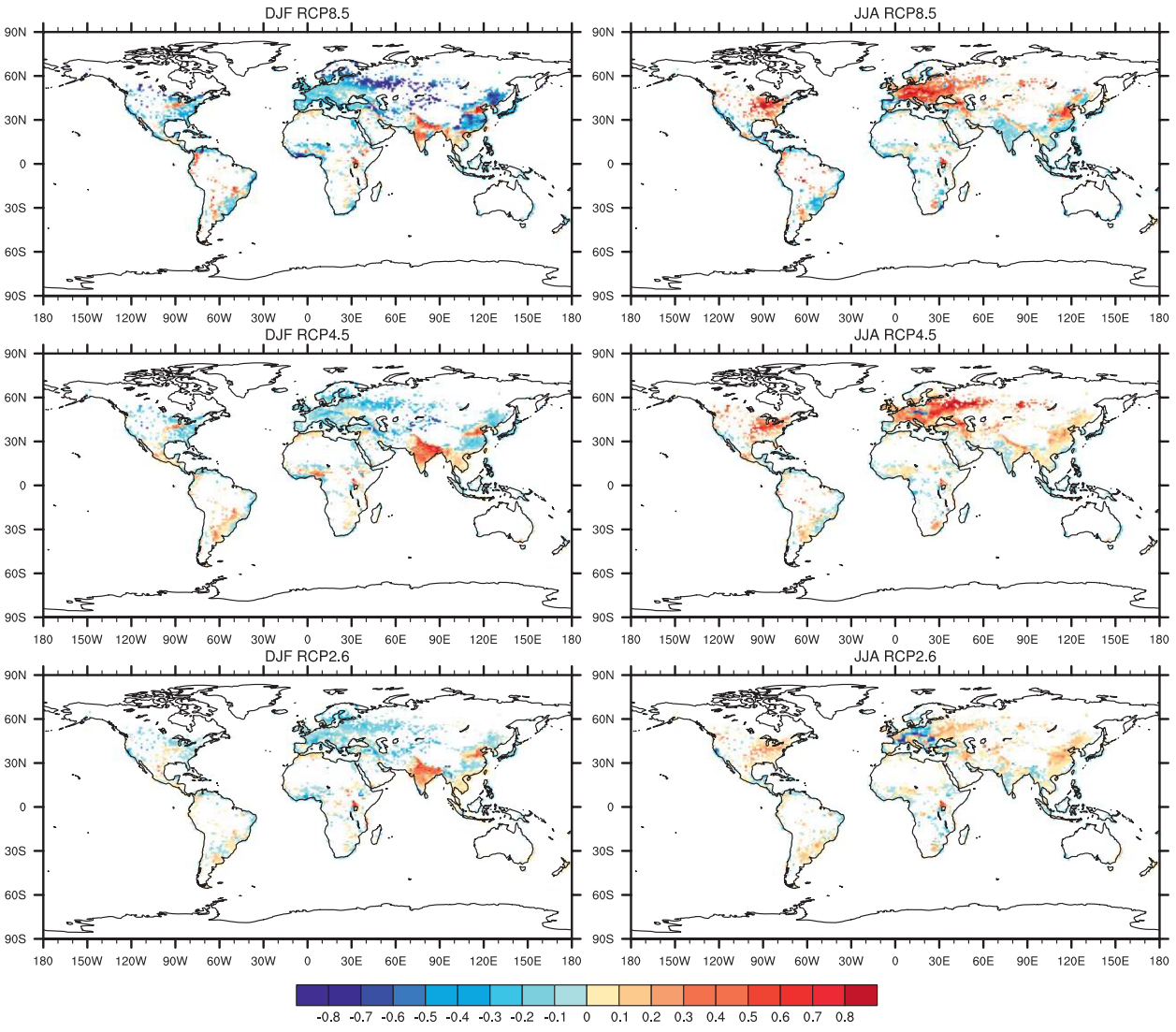

FIG. 7. As in Fig. 5, but for the urban minus rural daily minimum air temperature (nocturnal heat island).

2010). Another reason is that the same internal building maximum and minimum temperature settings are used for the entire urban area within a given geographic region (Jackson et al. 2010). In reality, building thermostat settings are more efficiently managed according to occupancy and building and environmental loads (Sailor 2010).

e. Attribution of changes in the heat island

In RCP8.5, the globally averaged UHI decreases by 0.07°C by the end of the twenty-first century compared to present day (Table 1). Oleson et al. (2010a) reported a similar decrease in the UHI in the AR4 A2 scenario using CAM3.5–CLM3.5 (0.10°C). This was attributed to a mechanism by which urban and rural areas respond differently to increased longwave radiation from a warmer atmosphere, with urban nocturnal temperature warming less than rural temperature. Such a mechanism exists here as well; however, the response of the UHI, particularly the nocturnal UHI (Fig. 7), is more variable seasonally and spatially than in Oleson et al. (2010a), and thus additional processes appear to be acting here. In this section, I provide some physical explanations for changes in the UHI, focusing separately on the daytime and nocturnal UHI since they respond differently (e.g., Figs. 4e,f).

The decrease in the daytime UHI occurs nearly everywhere in all RCPs and seasons, although the magnitude of change declines with weaker radiative forcing (Fig. 6). Changes in atmospheric CO_2 not only affect the radiative properties of the atmosphere but also the rates of plant assimilation of CO_2 and water loss by transpiration through the plant stomata. Figure 9 shows the changes in boreal summer urban and rural evaporative

TABLE 3. Seasonal pattern correlations between the RCP simulations for 2080–99 minus 1986–2005 urban minus rural average (AVG), daily maximum (TMAX), and daily minimum (TMIN) air temperature (i.e., as shown in Figs. 5, 6, 7). All correlations are significant at the 1% level.

	AVG		
Season	RCP8.5:RCP4.5	RCP8.5:RCP2.6	RCP4.5:RCP2.6
DJF	0.79	0.63	0.73
JJA	0.61	0.18	0.41
	TMAX		
Season	RCP8.5:RCP4.5	RCP8.5:RCP2.6	RCP4.5:RCP2.6
DJF	0.76	0.51	0.56
JJA	0.76	0.44	0.55
	TMIN		
Season	RCP8.5:RCP4.5	RCP8.5:RCP2.6	RCP4.5:RCP2.6
DJF	0.82	0.66	0.77
JJA	0.58	0.21	0.40

fraction (the ratio of latent heat flux to the sum of latent and sensible heat flux) in RCP8.5. Rural evaporative fraction decreases almost everywhere. In contrast to the rural response, the urban areas here appear to respond mainly to precipitation. For example, urban evaporative fraction increases in eastern China, Indochina, and India in response to an increase in precipitation. Rural evaporative fraction decreases despite increased precipitation so that urban minus rural evaporative fraction increases. Rural TMAX warms more than urban TMAX resulting in a relatively large decrease in the daytime UHI (Fig. 9). This can be seen clearly in the average diurnal cycles for southeastern China shown in Fig. 10. At midday, urban latent heat flux increases by about 30 W m^{-2} by the end of the century compared to present day, while rural latent heat flux decreases by about 20 W m^{-2}, with the energy partitioned to sensible heat flux instead. This decreases the daytime UHI.

The decrease in rural evaporative fraction may be due in part to a simulated increase in water use efficiency (the ratio of photosynthesis to transpiration; Fig. 9). With higher atmospheric CO_2 concentrations stomatal conductance decreases and water loss decreases. However, stomata respond to other environmental variables as well. For example, changes in soil moisture, vapor pressure deficit, and the canopy light environment may modulate the response to elevated CO_2 (Wullschleger et al. 2002).

The pattern correlations between the change in JJA daytime UHI and urban minus rural evaporative fraction in RCP8.5, RCP4.5, and RCP2.6 are all $r = -0.68$. The correlations are weaker in boreal winter ($r = -0.56$, -0.48, and -0.56 in RCP8.5, RCP4.5, and RCP2.6, respectively). In the Southern Hemisphere, increases in the urban minus rural evaporative fraction do cause decreases in the daytime UHI (e.g., the strong decrease in Brazil for DJF RCP8.5 shown in Fig. 6). At higher latitudes in the Northern Hemisphere, however, evaporation in winter is small. Here, the UHI is maintained in part by building heat and associated wasteheat (Oleson et al. 2010a). As climate warms, less space heating is needed to keep buildings warm (Table 4). This results in a decrease in the UHI. For example, in Europe the energy required to keep the interior of the buildings warm (urban heat flux in Fig. 11) is about 12 W m^{-2} less by the end of the century compared to present day. Sensible heat flux is reduced accordingly so that urban air temperature warms less than the rural air temperature. Note that both the daytime and nocturnal UHI decrease.

McCarthy et al. (2010b) found a positive correlation between changes in the rural DTR and changes in the nocturnal UHI in a doubled CO_2 experiment using the HadAM3 global climate model, which explained 49% of the variance in the nocturnal UHI. A quite strong relation is found here as well, explaining 63%, 67%, and 80% of the change in the nocturnal UHI in RCP8.5, RCP4.5, and RCP2.6, respectively. The changes in the nocturnal UHI in Europe are particularly interesting because of the relatively large and spatially coherent increases in summer and decreases in winter in RCP8.5 (Fig. 7). In contrast, there are significant parts of Europe with reductions in the summer nocturnal UHI in RCP2.6.

In summer in RCP8.5, changes in rural DTR are strongly negatively correlated with changes in clouds and rural soil moisture and positively correlated with leaf plus stem area index (lsai) (as indicated by the simple correlation coefficients in Table 5). The corresponding simple correlations for the nocturnal UHI are of the same sign but somewhat weaker for clouds and stronger for lsai. When the effects of the other variables are held constant in the multiple regression analysis (the standardized partial regression coefficients in Table 5), the results indicate that clouds and lsai are most important in determining changes in rural DTR and lsai is the most important in the nocturnal UHI relative to other variables. Clouds are negatively correlated with DTR because they reflect sunlight and reduce TMAX (Dai et al. 1999).

Large increases in rural DTR and the nocturnal UHI are associated with large increases in lsai (Fig. 12), with correlation coefficients of $r = 0.69$ and $r = 0.80$, respectively (Table 5). Increases in lsai can affect both TMAX and TMIN (Jeong et al. 2011). Increased lsai may decrease TMAX through increased evapotranspiration and the influence of evapotranspiration on cloudiness and precipitation (Collatz et al. 2000). However, the

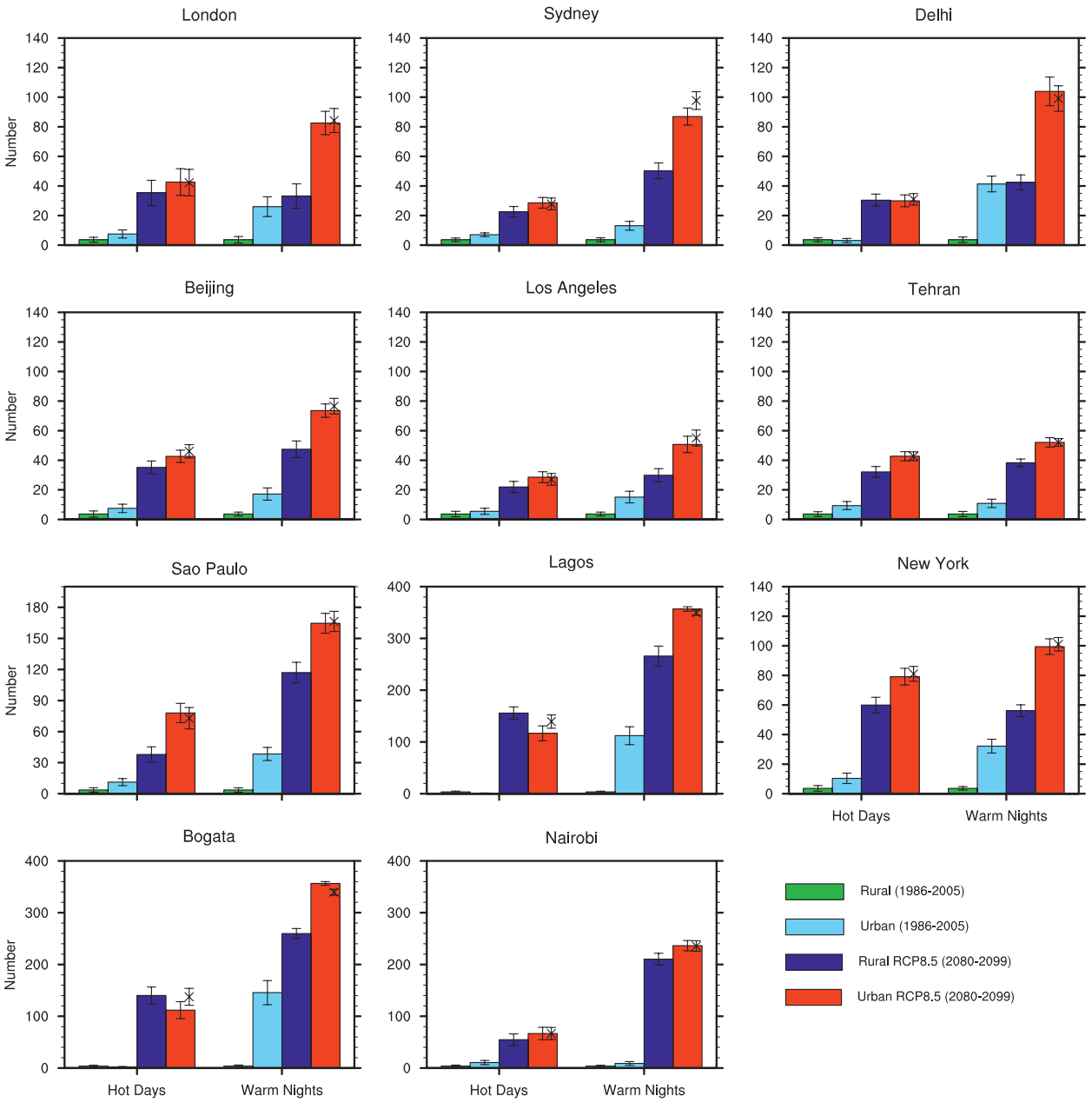

FIG. 8. Average annual frequency of hot days and warm nights for selected cities for 1986–2005 of the twentieth-century simulation and 2080–99 of the RCP8.5 simulation for urban and rural areas. Hot days are defined as the number of days that the daily maximum air temperature exceeds the 99th percentile of the 1986–2005 rural daily maximum air temperature. Warm nights are defined similarly using the daily minimum air temperature. Crosses indicate the hot days/warm nights estimated by adding the 1986–2005 daytime/nocturnal heat island to the 2080–99 rural maximum/minimum temperature. Error bars represent the 95% confidence level of the estimated average annual frequency. Data are from hourly output of one ensemble member each of the twentieth-century and RCP8.5 simulations.

degree to which this may occur depends on moisture availability. In Europe, cloudiness and rural soil moisture decreased (e.g., Fig. 12 for clouds), and precipitation and rural evaporative fraction decreased as well (Fig. 9). Larger lsai also shades soil during the day and reduces the amount of heat penetrating into the soil. Less heat is then released at night, which increases the cooling rate of the soil and decreases the nocturnal air temperature (Zhou et al. 2007). Here, the increase in lsai appears to limit increases in TMIN due to climate warming and has less of an effect on TMAX resulting in a strong positive correlation between lsai and rural DTR and the nocturnal UHI.

TABLE 4. Urban air conditioning (AC), space heating (HEAT), and wasteheat (WSTH) fluxes for present day (1986–2005) and end of the century (2080–99) in RCP8.5, RCP4.5, and RCP2.6 (all in terawatts).

		1986–2005	RCP8.5 2080–99	RCP4.5 2080–99	RCP2.6 2080–99
AC	Global	0.11	0.36	0.18	0.14
	20°–40°N	0.10	0.20	0.15	0.13
	40°–60°N	0.01	0.16	0.03	0.01
HEAT	Global	4.9	3.2	4.0	4.3
	20°–40°N	1.2	0.6	0.9	1.0
	40°–60°N	3.6	2.5	3.0	3.2
WSTH	Global	6.4	5.0	5.5	5.8
	20°–40°N	1.8	1.5	1.5	1.6
	40°–60°N	4.5	3.4	3.8	4.1

The changes in urban DTR have a pattern similar to rural DTR (Fig. 12) despite the fact that lsai is not relevant to the urban model since there is no vegetation in the urban area. This is because the rural surface is strongly coupled to the atmosphere while the urban surface is weakly coupled if at all. The rural changes feed back to the atmosphere and affect the atmosphere overlying the urban area. The urban TMIN shows a similar pattern to the rural TMIN in areas with large increases in lsai, though the response is muted because this is an indirect effect.

The simple correlation coefficients indicate that changes in lsai also strongly control changes in rural DTR and the nocturnal UHI in summer in RCP2.6 (Table 5 and Fig. 13). In this case, decreases in rural DTR and the nocturnal UHI are associated with decreases in lsai. Decreased lsai allows more radiation to be absorbed by the soil during daytime and released at night thereby increasing the rural nocturnal temperature. On the other hand, the partial regression coefficients indicate that lsai is more modestly correlated with rural DTR and the nocturnal UHI. Wind speed is strongly negatively correlated with rural DTR and the nocturnal UHI. Partial correlation analysis indicates that this is partly due to an indirect effect because of a negative correlation between wind and lsai ($r = -0.56$). Decreased lsai reduces drag on the atmosphere thereby increasing wind speed. However, the partial correlations of wind with rural DTR and the nocturnal UHI and with the effects of lsai removed are both $r = -0.57$. A significant negative regression coefficient is found in the regression model as well. An increase in wind speed can reduce the UHI because it promotes turbulence as a cooling process relative to that of radiation (Oke 1987). Changes in atmospheric stability may also contribute to the changes in wind speed. However, sensitivity experiments would be required to confirm whether such mechanisms are at work here.

The influence of lsai on the UHI in RCP8.5 and RCP2.6 is supported by recent research. Imhoff et al. (2010) found that ecological context influences the amplitude of summer daytime skin temperature defined UHI for U.S. cities. The largest UHIs were found for urban areas embedded in high biomass forested biomes and less intense UHIs in urban areas surrounded by shorter low biomass vegetation such as grassland, shrubland, and savannah. Zhang et al. (2010) extended this work globally and found similar ordering of UHIs by biomass.

In winter in RCP8.5, the simple correlation coefficients indicate that clouds exert a major control on changes in rural DTR (Table 5 and Fig. 14). There is an increase in clouds at northern latitudes that is associated with increases in rural TMIN, which reduces rural DTR. Rural TMIN is strongly positively correlated with clouds ($r = 0.77$) and even more so with downward longwave radiation associated with clouds ($r = 0.92$). Similarly, a decrease in clouds at southern latitudes is associated with an increase in rural DTR. Clouds are also strongly correlated with the nocturnal UHI, although the simple correlation is weaker than for rural DTR (Table 5). This is consistent with the fact that the nocturnal UHI is most well developed in clear-sky conditions and is reduced in cloudy conditions because clouds diminish the nocturnal radiative cooling differences between rural and urban areas (Oke 1987).

Rural soil moisture appears to play a role as well. Rural DTR and the nocturnal UHI are strongly negatively correlated with soil moisture (Table 5 and Fig. 14). Soil moisture affects the thermal admittance of the soil and therefore the diurnal cycle of heat storage. Drier soils cool off faster at night than wet soils because less heat is released from the soil. Rural soil moisture is therefore inversely related to rural DTR and the nocturnal UHI. The increase in soil moisture at northern latitudes could contribute to a decrease in rural DTR and the nocturnal UHI by increasing the thermal admittance of the soil. The partial regression coefficients in Table 5 indicate that clouds have a stronger effect than rural soil moisture on rural DTR in winter. Conversely, rural soil moisture is much more strongly correlated with the nocturnal UHI than clouds are. However, rural soil moisture and clouds are strongly correlated with each other ($r = 0.70$) making it difficult for the regression model to separate their effects.

6. Summary and conclusions

Version 4 of the Community Climate System Model (CCSM4) includes a new parameterization of urban areas in addition to its parameterization of vegetated (rural)

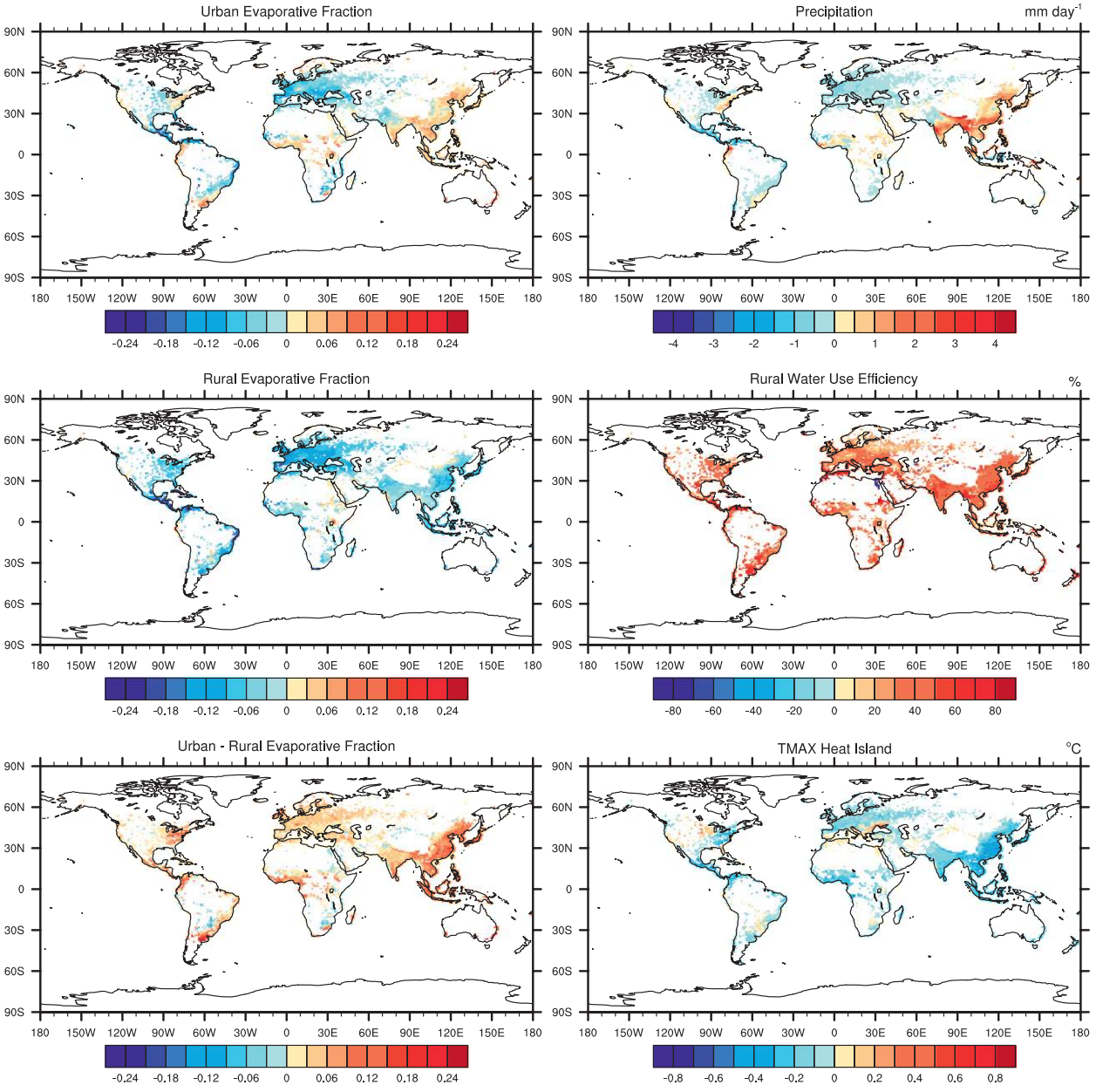

FIG. 9. Change (RCP8.5 2080–2099 minus 1986–2005) in JJA (left, top to bottom) urban, rural, and urban minus rural evaporative fraction and (right, top to bottom) precipitation, rural water use efficiency (in percent), and the daytime heat island. Water use efficiency is calculated as A/E where A is photosynthesis (moles CO_2 fixed), and E is transpiration (moles H_2O).

surfaces. CCSM4 simulations of present day and future climate have been performed in support of the IPCC AR5 as part of the Coupled Model Intercomparison Project (CMIP5). These include a set of twentieth-century simulations that provide a baseline present day climate and three sets of simulations of future climate scenarios (representative concentration pathways; RCP8.5, RCP4.5, and RCP2.6). These simulations were analyzed to examine how rural and urban areas might respond differently to changes in climate. In particular, changes in the urban heat island (UHI) are an indication of this response.

The UHI is defined here as the difference between the urban and rural air temperatures in each grid cell. This difference was analyzed for daily average (AVG), daily maximum (TMAX), and daily minimum (TMIN) temperature. The latter two are also referred to as the daytime and nocturnal UHIs, respectively. Globally averaged, urban and rural air temperature both increase in the

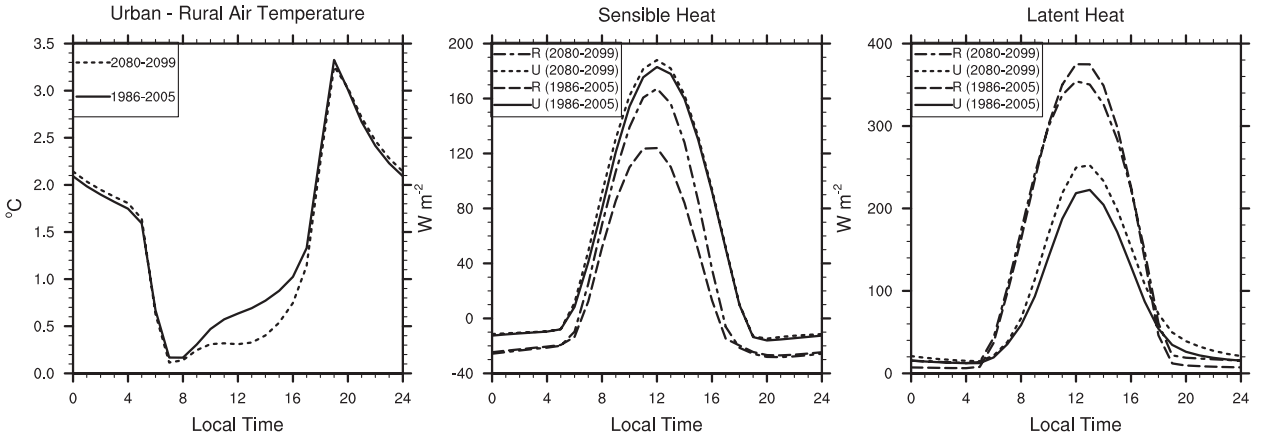

FIG. 10. Average JJA diurnal cycle of (left to right) urban minus rural air temperature, and urban (*U*) and rural (*R*) sensible and latent heat flux for southeastern China (23°–37°N, 105°–122°E) for 1986–2005 and 2080–99. Data are from hourly output of one ensemble member each of the twentieth-century and RCP8.5 simulations.

future, the magnitude of the response being ordered by degree of radiative forcing in the future scenarios. The AVG UHI at the end of the twenty-first century is similar to present day in RCP4.5 and RCP2.6 and decreases in RCP8.5 (0.07°C). The daytime UHI decreases in all scenarios; again with the response ordered by radiative forcing (e.g., by a maximum of 0.13°C in RCP8.5). The nocturnal UHI at the end of the twenty-first century is similar to present day in RCP2.6 and RCP4.5 and decreases in RCP8.5.

The decrease in the daytime UHI is quite uniform across regions and seasons and is shown to be due mainly to contrasts between changes in urban and rural evaporative fraction. Rural evaporative fraction decreases almost everywhere because of the increased water use efficiency under higher CO_2 concentrations. In contrast, the urban areas here are not affected by CO_2 and respond mainly to precipitation. The net effect is an increase in urban minus rural evaporative fraction which results in a decrease in the daytime UHI.

In contrast to the changes in the daytime UHI, there is significant spatial and seasonal variability in the response of the nocturnal UHI. Changes in the rural diurnal temperature range (DTR) were found to be a good predictor of changes in the nocturnal UHI, with decreases in the rural DTR corresponding to decreases in the nocturnal UHI, confirming the results of McCarthy et al. (2010b). Thus, it is primarily the response of rural temperature that is causing the changes in the nocturnal UHI. Variability in the response of Europe's nocturnal UHI was examined in detail to identify the main processes responsible. Changes in rural leaf plus stem area

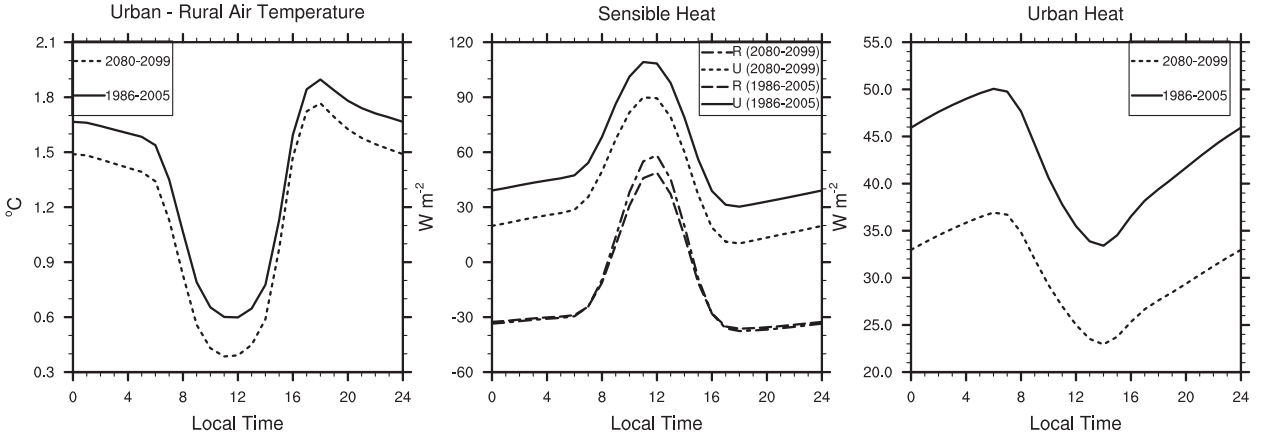

FIG. 11. Average DJF diurnal cycle of (left to right) urban minus rural air temperature, urban (*U*) and rural (*R*) sensible heat flux, and urban heat flux for Europe (37°–60°N, 10°W°–30°E) for 1986–2005 and 2080–99. Urban heat is the flux required to maintain interior building temperatures above a prescribed comfort level. Data are from hourly output of one ensemble member each of the twentieth-century and RCP8.5 simulations.

TABLE 5. Simple (S) and standardized partial regression coefficients (P) between changes (2080–99 minus 1986–2005) in rural diurnal temperature range [dtr(r)] and nocturnal heat island (tmin hi), and humidity (q), wind speed (w), total cloud fraction (tc), leaf plus stem area index (lsai), soil moisture [$b(r)$, $b(u)$], and urban wasteheat (wh) over Europe (35°–60°N, 10°W–60°E). The variable $b(r)$ for the rural surface is an indication of soil moisture stress affecting plant transpiration used here as a surrogate for soil moisture, while $b(u)$ is an indication of soil moisture stress for the urban pervious canyon floor. The R^2 is the percentage of variance explained by the regression model. Only grid cells that contain urban areas are included in the analysis (as shown in Fig. 7). Numbers in boldface are significant at the 1% level.

	JJA RCP8.5				JJA RCP2.6				DJF RCP8.5			
	dtr(r)		tmin hi		dtr(r)		tmin hi		dtr(r)		tmin hi	
	S	P	S	P	S	P	S	P	S	P	S	P
q	**−0.28**	**0.15**	**−0.29**	**−0.07**	**0.25**	**−0.21**	**0.27**	**−0.17**	−0.04	**−0.11**	**−0.12**	**−0.10**
w	**−0.20**	**0.10**	**−0.33**	**−0.09**	**−0.73**	**−0.51**	**−0.73**	**−0.43**	**−0.50**	**−0.10**	**−0.28**	**0.12**
tc	**−0.67**	**−0.56**	**−0.45**	**−0.11**	**0.48**	**0.07**	**0.52**	0.05	**−0.89**	**−0.67**	**−0.57**	**−0.17**
lsai	**0.69**	**0.57**	**0.80**	**0.68**	**0.74**	**0.43**	**0.79**	**0.50**	−0.03	**0.26**	−0.01	**0.38**
$b(r)$	**−0.40**	**−0.15**	**−0.36**	**−0.13**	**−0.40**	**−0.18**	**−0.39**	**−0.17**	**−0.78**	**−0.37**	**−0.53**	**−0.91**
$b(u)$	—	—	**−0.31**	**−0.12**	—	—	**0.54**	0.07	—	—	**−0.52**	**0.16**
wh	—	—	0.07	**0.10**	—	—	0.00	**0.10**	—	—	**0.14**	**0.16**
R^2	—	**78**	—	**74**	—	**75**	—	**80**	—	**93**	—	**70**

index in summer and in clouds and rural soil moisture in winter explained the majority of this variability. It should be noted that the DTR simulated by climate models is generally much weaker than observed (Randall et al. 2007). In part this may be related to poor simulation of the stable boundary layer (Holtslag 2006). This could contribute to an underestimate of changes in DTR (Zhou et al. 2009) and therefore the nocturnal UHI.

Changes in the frequency of hot days and warm nights for urban and rural areas were examined in RCP8.5. The analysis confirms results of McCarthy et al. (2010a) that climate change increases the number of warm nights in

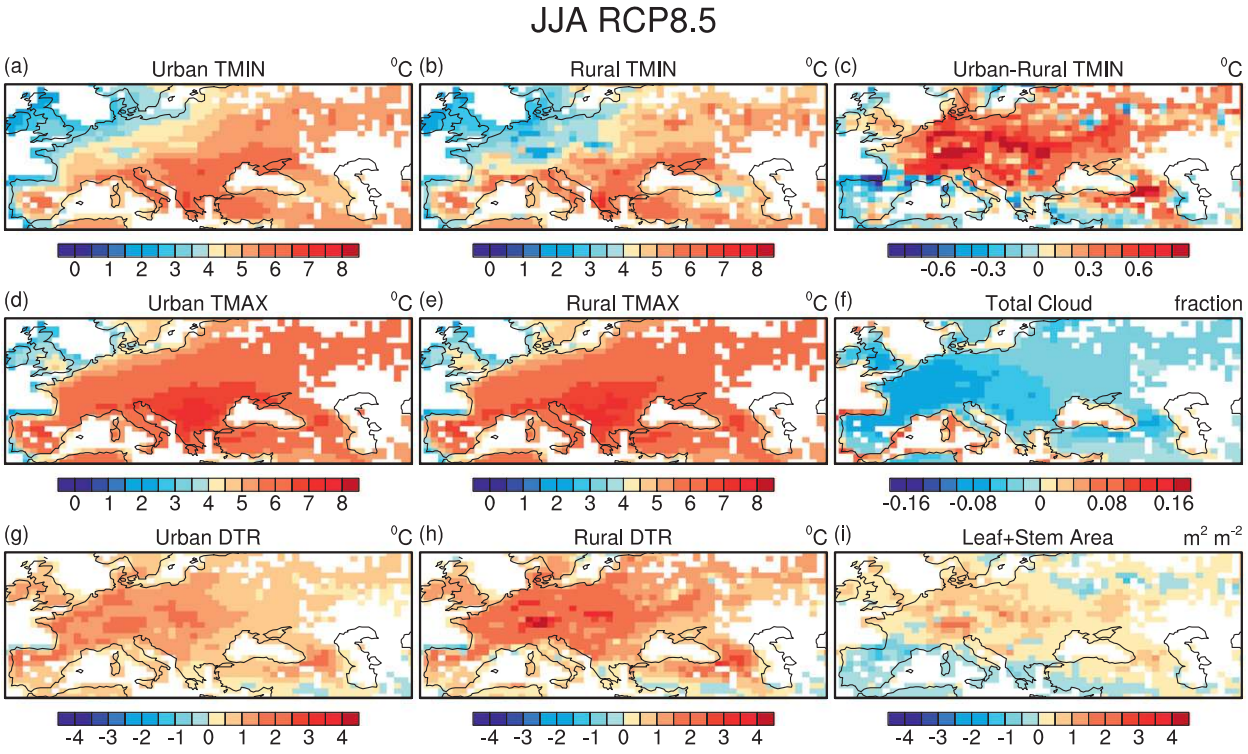

FIG. 12. Change (2080–99 minus 1986–2005) in (a) urban daily minimum temperature (TMIN), (b) rural TMIN, (c) urban minus rural TMIN, (d) urban daily maximum temperature (TMAX), (e) rural TMAX, (f) total cloud, (g) urban diurnal temperature range (DTR), (h) rural DTR, and (i) leaf plus stem area for JJA RCP8.5 in Europe (35°–50°N, 10°E–60°W).

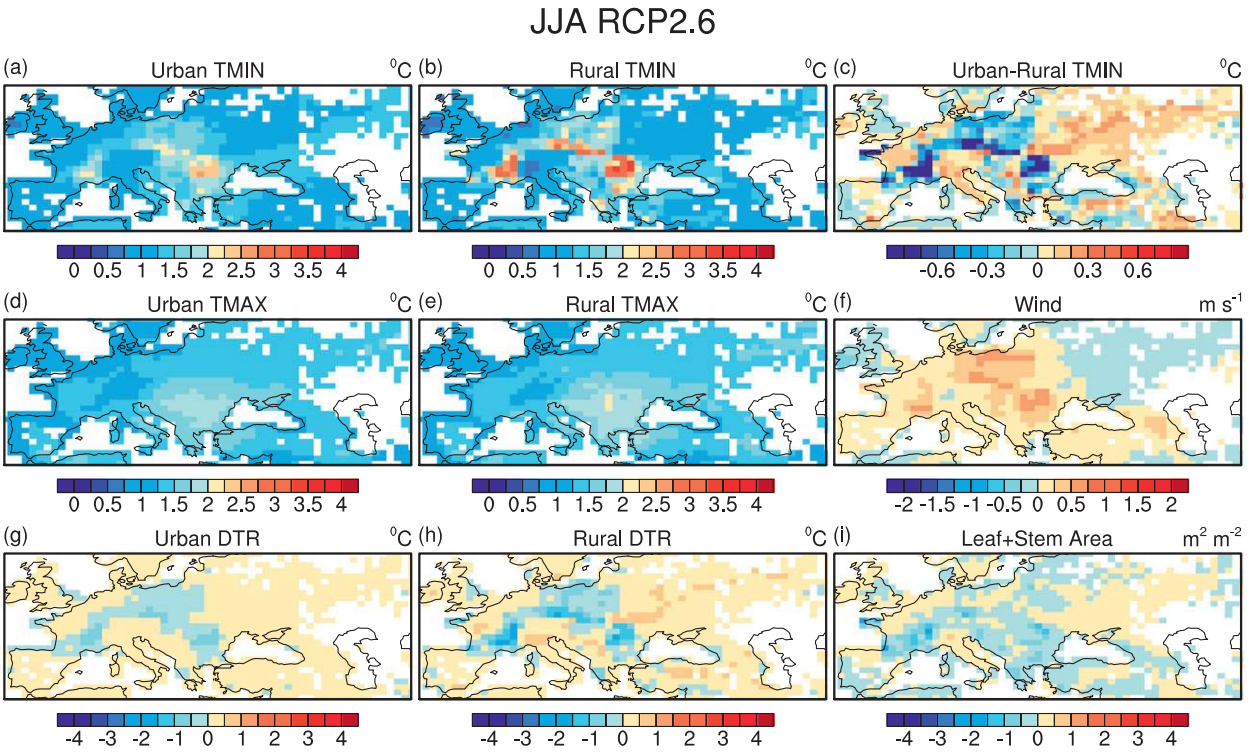

FIG. 13. As in Fig. 12, but for JJA RCP2.6 and with (f) wind instead of total cloud.

urban areas substantially more than in rural areas. This is clearly a direct consequence of urban areas being warmer at night than rural areas, but it was also confirmed that the number of urban hot nights cannot be accurately estimated by linearly adding the present day UHI to rural future climate. Air conditioning flux increased and space heating decreased as climate warmed. In colder climates in winter, the UHI is maintained in part by building heat and associated wasteheat. As climate warms, less space heating is needed to keep buildings warm, contributing to a decrease in the UHI.

Oleson et al. (2010a) discussed several limitations of modeling urban and rural climate within global climate models, mainly related to the coarse spatial resolution of the model and inadequacies of datasets. These limitations apply to the current study as well, but several of these as well as other limitations merit further discussion here.

The urban representation is currently limited to a single medium density urban landunit in each grid cell. It has been shown that urban density is a major driving factor in determining the magnitude of the UHI. For instance, Oke (1981) showed that the strength of the maximum UHI is positively linearly correlated with height to width ratio, one measure of urban density. Coutts et al. (2007) found greater urban nocturnal temperatures with increasing urban density due in part to canyon morphology. Implementing other urban density types available in the Jackson et al. (2010) dataset (e.g., tall building district and high density) within the model would likely produce larger present day UHIs because of larger height to width ratios and smaller pervious area. These urban density types may have different responses to changes in climate. For example, anthropogenic heating due to space heating and air conditioning (HAC) processes is generally largest in the urban core (Sailor and Lu 2004) and thus the UHI may be more sensitive to changes in climate. The model structure should be expanded to other density types to explore the robustness of these results with respect to urban density. In addition, the lack of changes in urban extent and properties in the model was noted in section 5a as a limitation in modeling future changes in the UHI. Datasets of future urban extent and properties need to be developed and tested.

In this modeling framework the urban and rural areas within a given grid cell are forced by the same atmosphere and so share the same boundary layer. By not representing the differences between urban and rural boundary layers the model cannot capture mesoscale processes that affect the UHI, including boundary layer stability differences and boundary layer properties that force the urban and rural surfaces (e.g., downwelling solar and longwave radiation differences due to urban pollution) (Oke 1987). Other mesoscale processes related

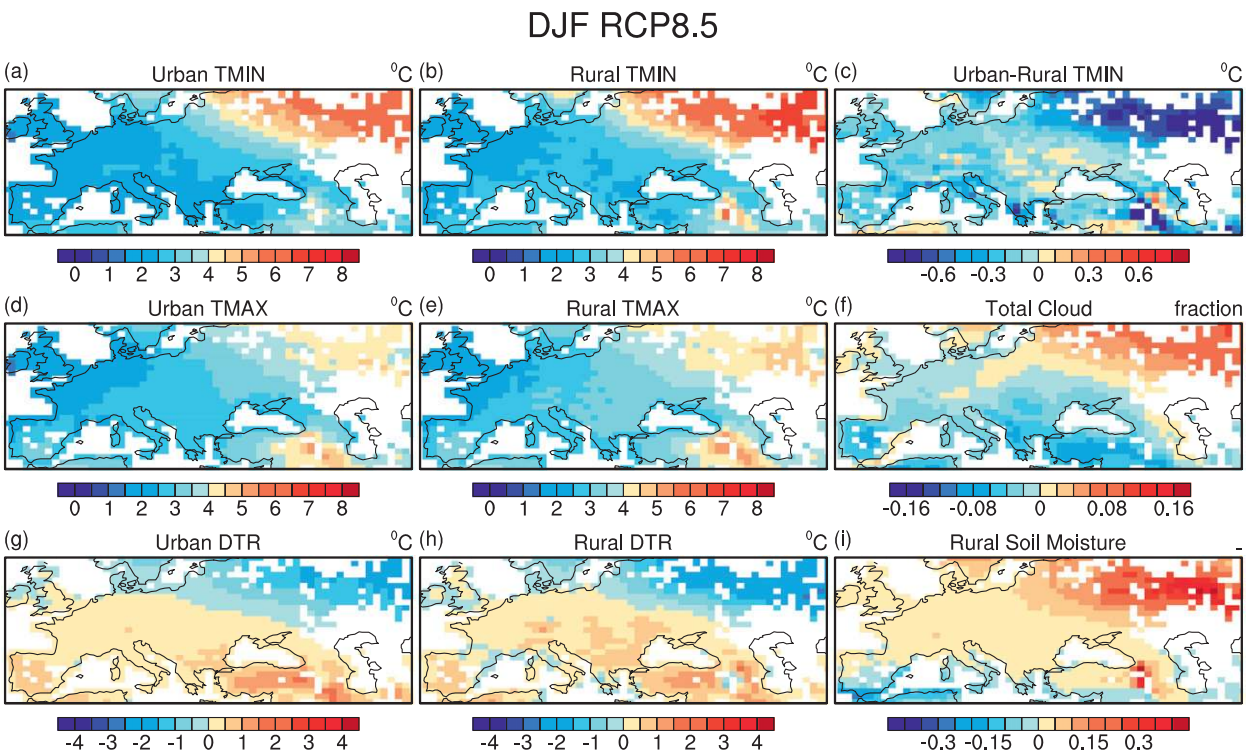

FIG. 14. As in Fig. 12, but for DJF RCP8.5 and with (i) rural soil moisture instead of leaf plus stem area.

to urban–rural interactions such as the urban heat island circulation are also not captured. Furthermore, the urban areas are small with respect to the size of the grid cell and so do not affect the overlying atmosphere.

The simulated urban climate is also affected by estimates of wasteheat from the model. Since the wasteheat is tied to the HAC fluxes, uncertainties in these fluxes propagate to the estimates of wasteheat, which in turn affect urban air temperature. Incomplete knowledge of building temperature settings and thermal properties that control building thermal loads as well as variations in the efficiencies of HAC systems contribute to uncertainties in these fluxes. In addition, other sources of wasteheat such as traffic and internal sources of building heat (human metabolism and equipment and potential changes in these over time) (Sailor 2010) are neglected here. An additional uncertainty is that all wasteheat is assumed to be in the form of sensible heat although certain types of mechanical equipment such as cooling towers may emit more moisture than sensible heat (Sailor 2010). Sensitivity analysis of these fluxes with respect to climate change is a topic for future research (e.g., McCarthy et al. 2010a).

Given the limitations and uncertainties discussed here, these results should not be considered as projections of future climate change in urban areas. Instead, these results highlight a number of ways in which urban and rural areas can respond differently to climate change. A key example highlighted here is the significant increase in the summer nocturnal UHI in Europe under RCP8.5. This is attributed to increased leaf–stem area of the rural surface which keeps the rural surface cooler than it would otherwise be under climate warming. The urban area does not benefit from this mechanism and so the UHI increases. This suggests that increasing vegetation within cities may be one way of counteracting warming, an approach suggested by other studies (e.g., Rosenzweig et al. 2009).

Thus, the unique aspects of the urban environment should be considered when making projections about the effects of climate change, particularly since the global population is becoming increasingly urbanized. Preferably, urban areas will be included explicitly in models of climate change since urban–rural contrasts cannot necessarily be determined from present-day patterns. The importance of this is underscored by the fact that the differences in the response of urban and rural areas are likely underestimated here given the limitations mentioned above. In particular, the expanding urban population and its influence on urban development are likely to be a significant control on the UHI in the future.

Acknowledgments. This research was supported in part by the NCAR Weather and Climate Impacts Assessment

Program. Thanks are due to the software engineers and scientists who contributed to the development of CCSM4 and executed the simulations described here. I would also like to acknowledge the significant contributions of Erik Kluzek, the primary CLM software engineer. Three anonymous reviewers are thanked for their thorough reviews that led to substantial improvements in the manuscript. The CCSM project is supported by the National Science Foundation and the Office of Science (BER) of the U.S. Department of Energy. Computing resources were provided by the Climate Simulation Laboratory at NCAR's Computational and Information Systems Laboratory (CISL), sponsored by the National Science Foundation and other agencies. This research was enabled by CISL compute and storage resources. Bluefire, a 4064-processor IBM Power6 resource with a peak of 77 TeraFLOPS provided more than 7.5 million computing hours, the GLADE high-speed disk resources provided 0.4 PetaBytes of dedicated disk, and CISL's 12-PB HPSS archive provided over 1 PetaByte of storage in support of this research project. NCAR is sponsored by the National Science Foundation.

REFERENCES

Allen, L., F. Lindberg, and C. S. B. Grimmond, 2011: Global to city scale urban anthropogenic heat flux: Model and variability. *Int. J. Climatol.,* **31,** 1990–2005, doi:10.1002/joc.2210.

Anderson, T. W., 2003: *An Introduction to Multivariate Statistical Analysis*. 3rd ed. John Wiley and Sons, Inc., 721 pp.

Arnfield, A. J., 2003: Two decades of urban climate research: A review of turbulence, exchanges of energy and water, and the urban heat island. *Int. J. Climatol.,* **23,** 1–26, doi:10.1002/joc.859.

Best, M. J., C. S. B. Grimmond, and M. G. Villani, 2006: Evaluation of the urban tile in MOSES using surface energy balance observations. *Bound.-Layer Meteor.,* **118,** 503–525, doi:10.1007/s10546-005-9025-5.

Bettencourt, L., and G. West, 2010: A unified theory of urban living. *Nature,* **467,** 912–913.

Bornstein, R. D., 1975: The two-dimensional URBMET urban boundary layer model. *J. Appl. Meteor.,* **14,** 1459–1477.

——, 1986: Urban climate models: Nature, limitations, and applications. *Urban Climatology and its Applications with Special Regard to Tropical Areas,* T. R. Oke, Ed., WMO 652, World Meteorological Organization, 237–276.

Brown, M., 2000: Urban parameterizations for mesoscale meteorological models. *Mesoscale Atmospheric Dispersion,* Z. Boybeyi, Ed., WIT Press, 193–255.

Chen, F., and Coauthors, 2010: The integrated WRF/urban modeling system: Development, evaluation, and applications to urban environmental problems. *Int. J. Climatol.,* **31,** 273–288, doi:10.1002/joc.2158.

Collatz, G. J., L. Bounoua, S. O. Los, D. A. Randall, I. Y. Fung, and P. J. Sellers, 2000: A mechanism for the influence of vegetation on the response of the diurnal temperature range to changing climate. *Geophys. Res. Lett.,* **27,** 3381–3384.

Collier, C. G., 2006: The impact of urban areas on weather. *Quart. J. Roy. Meteor. Soc.,* **132,** 1–25, doi:10.1256/qj.05.199.

Coutts, A. M., J. Beringer, and N. J. Tapper, 2007: Impact of increasing urban density on local climate: Spatial and temporal variations in the surface energy balance in Melbourne, Australia. *J. Appl. Meteor. Climatol.,* **46,** 477–493.

——, ——, and ——, 2010: Changing urban climate and CO_2 emissions: Implications for the development of policies for sustainable cities. *Urban Policy Res.,* **28,** 27–47, doi:10.1080/08111140903437716.

Dai, A., K. E. Trenberth, and T. R. Karl, 1999: Effects of clouds, soil moisture, precipitation, and water vapor on diurnal temperature range. *J. Climate,* **12,** 2451–2473.

Danabasoglu, G., S. Bates, B. P. Briegleb, S. R. Jayne, M. Jochum, W. G. Large, S. Peacock, and S. G. Yeager, 2012: The CCSM4 ocean component. *J. Climate,* in press.

Energy Information Administration, cited 2008: 2003 commercial buildings energy consumption survey, energy end-use consumption Table E1A. [Available online at http://www.eia.doe.gov/emeu/consumption/index.html.]

——, cited 2009: 2005 residential energy consumption survey, energy consumption and expenditures Table US11. [Available online at http://www.eia.doe.gov/emeu/consumption/index.html.]

Flanner, M. G., 2009: Integrating anthropogenic heat flux with global climate models. *Geophys. Res. Lett.,* **36,** L02801, doi:10.1029/2008GL036465.

Fortuniak, K., K. Klysik, and J. Wibig, 2005: Urban-rural contrasts of meteorological parameters in Łódź. *Theor. Appl. Climatol.,* **84,** 91–101.

Gent, P. R., and Coauthors, 2011: The Community Climate System Model version 4. *J. Climate,* **24,** 4973–4991.

Golden, J. S., 2004: The built environment induced urban heat island effect in rapidly urbanizing arid regions—A sustainable urban engineering complexity. *J. Integr. Environ. Sci.,* **1,** 321–349.

Gosling, S. N., J. A. Lowe, G. R. McGregor, M. Pelling, and B. D. Malamud, 2009: Associations between elevated atmospheric temperature and human mortality: A critical review of the literature. *Climatic Change,* **92,** 299–341.

Grimmond, C. S. B., and Coauthors, 2010: The international urban energy balance models comparison project: First results from phase 1. *J. Appl. Meteor. Climatol.,* **49,** 1268–1292.

——, and Coauthors, 2011: Initial results from phase 2 of the international urban energy balance model comparison. *Int. J. Climatol.,* **31,** 244–272.

Hadley, S. W., D. J. Erickson III, J. L. Hernandez , C. T. Broniak, and T. J. Blasing, 2006: Responses of energy use to climate change: A climate modeling study. *Geophys. Res. Lett.,* **33,** L17703, doi:10.1029/2006GL026652.

Hansen, J., R. Ruedy, M. Sato, M. Imhoff, W. Lawrence, D. Easterling, T. Peterson, and T. Karl, 2001: A closer look at United States and global surface temperature change. *J. Geophys. Res.,* **106,** 23 947–23 963.

Holland, M. M., D. A. Bailey, B. P. Briegleb, B. Light, and E. Hunke, 2012: Improved sea ice shortwave radiation physics in CCSM4: The impact of melt ponds and aerosols on Arctic sea ice. *J. Climate,* **25,** 1413–1430.

Holtslag, B., 2006: GEWEX Atmospheric Boundary-Layer Study (GABLS) on stable boundary layers. *Bound.-Layer Meteor.,* **118,** 243–246.

Hunke, E. C., and W. H. Lipscomb, 2008: CICE: The Los Alamos sea ice model, documentation and software, version 4.0. Los Alamos National Laboratory Tech. Rep. LA-CC-06-012, 72 pp. [Available online at http://oceans11.lanl.gov/trac/CISM/export/51/trunk/cism/doc/cicedoc.pdf.]

Hunt, J. C. R., M. Maslin, T. Killeen, P. Backlund, and H. J. Schellnhuber, 2007: Introduction. Climate change and urban areas: Research dialogue in a policy framework. *Philos. Trans. Roy. Soc.,* **365A,** 2615–2629, doi:10.1098/rsta.2007.2089.

Ichinose, T., K. Shimodozono, and K. Hanaki, 1999: Impact of anthropogenic heat on urban climate in Tokyo. *Atmos. Environ.,* **33,** 3897–3909.

Imhoff, M. L., P. Zhang, R. E. Wolfe, and L. Bounoua, 2010: Remote sensing of the urban heat island effect across biomes in the continental USA. *Remote Sens. Environ.,* **114,** 504–513, doi:10.1016/j.rse.2009.10.008.

Jackson, T. L., J. J. Feddema, K. W. Oleson, G. B. Bonan, and J. T. Bauer, 2010: Parameterization of urban characteristics for global climate modeling. *Ann. Assoc. Amer. Geogr.,* **100,** 848–865, doi:10.1080/00045608.2010.497328.

Jeong, S.-J., C.-H. Ho, T.-W. Park, J. Kim, and S. Levis, 2011: Impact of vegetation feedback on the temperature and its diurnal range over the Northern Hemisphere during summer in a 2 x CO_2 climate. *Climate Dyn.,* **37,** 821–833, doi:10.1007/s00382-010-0827-x.

Karl, T. R., H. F. Diaz, and G. Kukla, 1988: Urbanization: Its detection and effect in the United States climate record. *J. Climate,* **1,** 1099–1123.

Klysik, K., and K. Fortuniak, 1999: Temporal and spatial characteristics of the urban heat island of Łódź, Poland. *Atmos. Environ.,* **33,** 3885–3895.

Landsberg, H. E., 1981: *The Urban Climate*. International Geophysical Series, Vol. 28, Academic Press, 275 pp.

Lawrence, D. M., and Coauthors, 2011: Parameterization improvements and functional and structural advances in version 4 of the Community Land Model. *J. Adv. Model. Earth Syst.,* **3,** doi:10.1029/2011MS000045.

——, K. W. Oleson, M. G. Flanner, C. G. Fletcher, P. J. Lawrence, S. Levis, S. C. Swenson, and G. B. Bonan, 2012: The CCSM4 land simulation, 1850–2005: Assessment of surface climate and new capabilities. *J. Climate,* in press.

Martilli, A., A. Clappier, and M. W. Rotach, 2002: An urban surface exchange parameterization for mesoscale models. *Bound.-Layer Meteor.,* **104,** 261–304.

Masson, V., 2000: A physically-based scheme for the urban energy budget in atmospheric models. *Bound.-Layer Meteor.,* **94,** 357–397.

——, 2006: Urban surface modeling and the meso-scale impact of cities. *Theor. Appl. Climatol.,* **84,** 35–45, doi:10.1007/s00704-005-0142-3.

McCarthy, M. P., M. J. Best, and R. A. Betts, 2010a: Climate change in cities due to global warming and urban effects. *Geophys. Res. Lett.,* **37,** L09705, doi:10.1029/2010GL042845.

——, ——, and ——, 2010b: Including cities in Met Office Hadley Centre global and regional climate projections. *Urban Climate News,* **36,** 5–8.

Meehl, G. A., and Coauthors, 2007: Global climate projections. *Climate Change 2007: The Physical Science Basis,* S. Solomon et al., Eds., Cambridge University Press, 747–845.

Mills, G., 1997: An urban canopy-layer climate model. *Theor. Appl. Climatol.,* **57,** 229–244.

Moss, R. H., and Coauthors, 2010: The next generation of scenarios for climate change research and assessment. *Nature,* **463,** 747–756, doi:10.1038/nature08823.

Myrup, L. O., 1969: A numerical model of the urban heat island. *J. Appl. Meteor.,* **8,** 908–918.

Neale, R. B., and Coauthors, 2011: Description of the NCAR Community Atmosphere Model (CAM4). NCAR Tech. Note NCAR/TN-485+STR, 212 pp. [Available online at http://www.cesm.ucar.edu/models/ccsm4.0/cam/docs/description/cam4_desc.pdf.]

Oke, T. R., 1981: Canyon geometry and the nocturnal urban heat island: Comparison of scale model and field observations. *J. Climatol.,* **1,** 237–254.

——, 1982: The energetic basis of the urban heat island. *Quart. J. Roy. Meteor. Soc.,* **108,** 1–24.

——, 1987: *Boundary Layer Climates*. 2nd ed. Routledge, 435 pp.

——, 1988: The urban energy balance. *Prog. Phys. Geogr.,* **12,** 471–508.

——, 1991: Climate of cities. *Climate in Human Perspective: A Tribute to Helmut E. Landsberg,* F. Baer, N. L. Canfield, and J. M. Mitchell, Eds., Kluwer Academic Publishers, 61–75.

——, 1997: Urban climates and global environmental change. *Applied Climatology: Principles and Practice,* R. D. Thompson and A. Perry, Eds., Routledge, 273–287.

——, and G. B. Maxwell, 1975: Urban heat island dynamics in Montreal and Vancouver. *Atmos. Environ.,* **9,** 191–200.

——, G. T. Johnson, D. G. Steyn, and I. D. Watson, 1991: Simulation of surface urban heat islands under ''ideal'' conditions at night. Part 2: Diagnosis of causation. *Bound.-Layer Meteor.,* **56,** 339–358.

Oleson, K. W., G. B. Bonan, J. Feddema, M. Vertenstein, and C. S. B. Grimmond, 2008a: An urban parameterization for a global climate model. Part I: Formulation and evaluation for two cities. *J. Appl. Meteor. Climatol.,* **47,** 1038–1060.

——, ——, ——, and —— , 2008b: An urban parameterization for a global climate model. Part II: Sensitivity to input parameters and the simulated urban heat island in offline simulations. *J. Appl. Meteor. Climatol.,* **47,** 1061–1076.

——, ——, ——, and T. Jackson, 2010a: An examination of urban heat island characteristics in a global climate model. *Int. J. Climatol.,* **31,** 1848–1865, doi:10.1002/joc.2201.

——, and Coauthors, 2010b: Technical description of version 4.0 of the Community Land Model (CLM). NCAR Tech. Note NCAR/TN-478+STR, 257 pp. [Available online at http://www.cesm.ucar.edu/models/cesm1.0/clm/CLM4_Tech_Note.pdf.]

——, G. B. Bonan, J. J. Feddema, M. Vertenstein, and E. Kluzek, 2010c: Technical description of an urban parameterization for the Community Land Model (CLMU). NCAR Tech. Note NCAR/TN-480+STR, 169 pp. [Available online at http://www.cesm.ucar.edu/models/cesm1.0/clm/CLMU_Tech_Note.pdf.]

Randall, D. A., and Coauthors, 2007: Climate models and their evaluation. *Climate Change 2007: The Physical Science Basis,* S. Solomon et al., Eds., Cambridge University Press, 589–662.

Rosenzweig, C., and Coauthors, 2009: Mitigating New York City's heat island: Integrating stakeholder perspectives and scientific evaluation. *Bull. Amer. Meteor. Soc.,* **90,** 1297–1312.

——, W. Solecki, S. A. Hammer, and S. Mehrotra, 2010: Cities lead the way in climate-change action. *Nature,* **467,** 909–911.

Roth, M., 2007: Review of urban climate research in (sub)tropical regions. *Int. J. Climatol.,* **27,** 1859–1873, doi:10.1002/joc.1591.

Sailor, D. J., 2010: A review of methods for estimating anthropogenic heat and moisture emissions in the urban environment. *Int. J. Climatol.,* **31,** 189–199, doi:10.1002/joc.2106.

——, and L. Lu, 2004: A top-down methodology for developing diurnal and seasonal anthropogenic heating profiles for urban areas. *Atmos. Environ.,* **38,** 2737–2748.

Scheitlin, K. N., and P. G. Dixon, 2010: Diurnal temperature range variability due to land cover and airmass types in the southeast. *J. Appl. Meteor. Climatol.,* **49,** 879–888.

Seto, K. C., and J. M. Shepherd, 2009: Global urban land-use trends and climate impacts. *Curr. Opin. Environ. Sustainability,* **1,** 89–95, doi:10.1016/j.cosust.2009.07.012.

Stone, B., Jr., 2007: Urban and rural temperature trends in proximity to large US cities: 1951-2000. *Int. J. Climatol.,* **27,** 1801–1807, doi:10.1002/joc.1555.

Taylor, K. E., R. J. Stouffer, and G. A. Meehl, 2009: A summary of the CMIP5 experiment design. World Climate Research Program, 32 pp. [Available at http://cmip-pcmdi.llnl.gov/cmip5/docs/Taylor_CMIP5_design.pdf.]

Trenberth, K. E., and Coauthors, 2007: Observations: Surface and atmospheric climate change. *Climate Change 2007: The Physical Science Basis,* S. Solomon et al., Eds, Cambridge University Press, 235–336.

United Nations, 2009: *World Urbanization Prospects, the 2009 Revision: Highlights*. Department of Economic and Social Affairs, Population Division, 47 pp.

Vautard, R., P. Yiou, and G. J. van Oldenborgh, 2009: Decline of fog, mist and haze in Europe over the past 30 years. *Nat. Geosci.,* **2,** 115–119.

Wienert, U., and W. Kuttler, 2005: The dependence of the urban heat island intensity on latitude—A statistical approach. *Meteor. Z.,* **14,** 677–686.

Wullschleger, S. D., C. A. Gunderson, P. J. Hanson, K. B. Wilson, and R. J. Norby, 2002: Sensitivity of stomatal and canopy conductance to elevated CO_2 concentration—Interacting variables and perspectives of scale. *New Phytol.,* **153,** 485–496.

Zhang, P., M. L. Imhoff, R. E. Wolfe, and L. Bounoua, 2010: Characterizing urban heat islands of global settlements using MODIS and nighttime lights products. *Can. J. Remote Sens.,* **36,** 185–196.

Zhou, L., R. E. Dickinson, Y. Tian, R. S. Vose, and Y. Dai, 2007: Impact of vegetation removal and soil aridation on diurnal temperature range in a semiarid region: Application to the Sahel. *Proc. Natl. Acad. Sci. USA,* **104,** 17 937–17 942.

——, ——, A. Dai, and P. Dirmeyer, 2009: Detection and attribution of anthropogenic forcing to diurnal temperature range changes from 1950 to 1999: Comparing multi-model simulations with observations. *Climate Dyn.,* **35,** 1289–1307, doi:10.1007/s00382-009-0644-2.